[redacted]

UNCLASSIFIED

SLA-74-0103

No Foreign

Analysis of the SIAM Infrared Acquisition System (U)

S. G. Varnado

Ernelda Seph 05/21/96 U — K.D Smith 96SN115

W C Hayes 6-13-96 — DATE 02-12-96

Prepared by Sandia Laboratories, Albuquerque, New Mexico 87115 and Livermore, California 94550 for the United States Atomic Energy Commission under Contract AT (29-1)-789

Printed February 1974

[redacted]

Classified by W. C. Hines, Supervisor, Div. 4733, Feb. 15, 1974

[redacted]

SANDIA SYSTEMATIC DECLASSIFICATION REVIEW

1st Review Date: 2-9-96
Authority: ☐ ADC ☒ ADD W Hayes
Name:

2nd Review Date: 2-9-96
Authority: ADD
Name: K.D. SMITH

Determination (Circle Numbers):
1. Classification Retained
2. Classification Changed to: U
3. Contains No DOE Classified Information
4. Coordinate With:
5. Contains UCAI?
6. Comments: Release

RECORD COPY

DO NOT TAKE FROM THIS ROOM

MASTER

by

[redacted]TRIBUTION OF THIS DOCUMENT IS UNLIMITED

[redacted] MICROFICHE

[redacted]

DISCLAIMER

Portions of this document may be illegible electronic image products. Images are produced from the best available original document.

Issued by Sandia Laboratories,
a prime contractor to the United States Atomic Energy Commission

[redacted]

UNCLASSIFIED

SLA-74-0103

ANALYSIS OF THE SIAM INFRARED ACQUISITION SYSTEM (U)

[redacted]

S. G. Varnado
Systems Studies Division, 4733
Sandia Laboratories, Albuquerque, NM 87115

Printed February 1974

ABSTRACT (U)

This report describes and presents the results of an analysis of the performance of the infrared acquisition system for a Self-Initiated Antiaircraft Missile (SIAM). A description of the optical system is included, and models of target radiant intensity, atmospheric transmission, and background radiance are given. Acquisition probabilities are expressed in terms of the system signal-to-noise ratio. System performance against aircraft and helicopter targets is analyzed, and background discrimination techniques are discussed.

[redacted]

[redacted]

UNCLASSIFIED

[redacted]

INTENTIONALLY LEFT BLANK

SUMMARY

Denial of the use of enemy aircraft in a European theatre war could provide an important tactical advantage to NATO forces. One concept for accomplishing this denial is the Self-Initiated Antiaircraft Missile (SIAM). SIAM is a remotely implanted, acoustically activated, automatic homing guided missile. In a typical scenario, missiles would be implanted near enemy airfields, probably by air drop. The system would be activated during aircraft takeoff by the acoustic signal from the aircraft. The missile would pop up and acquire the target with infrared techniques. It is proposed that terminal homing be accomplished with a Redeye-type seeker head.

The SIAM concept could provide a submarine defense against Soviet ASW helicopters. The missiles could be launched from a submerged submarine and subsequently deployed from the ocean surface. System activation and operation would then be similar to that described for the airfield denial scenario.

In this report, which establishes the feasibility of using infrared techniques for the target acquisition function, the following findings were obtained:

1. The 3.0 to 5.0 μ interval is the most promising wavelength band for operation of this system.

2. AGC-type logic is adequate for acquiring targets utilizing afterburner.

3. Background discrimination techniques must be employed to acquire targets utilizing cruise or military power.

4. Helicopter acquisition at a range of 4.5 km can be accomplished if effective background discrimination is employed.

5. Two-color discrimination is an effective technique which utilizes simple detection logic.

6. Additional data on the spectral radiance of various backgrounds are needed.

CONTENTS

LIST OF ILLUSTRATIONS

[redacted]

[redacted]

INTENTIONALLY LEFT BLANK

[redacted]

[redacted]

ANALYSIS OF THE SIAM INFRARED ACQUISITION SYSTEM

Introduction

Operation of Warsaw Pact tactical aircraft in a European theatre war may be from widely dispersed, temporary airfields. Some of these airfields may employ hardened aircraft shelters. Such procedures make it difficult for NATO forces to deny the use of enemy aircraft in a tactical situation. One concept for airfield denial is the Self-Initiated Antiaircraft Missile (SIAM), previously known as Little David.[1]

SIAM is a remotely implanted, ground-to-air, automatic homing, guided missile. In a typical scenario, the missiles would be "seeded" near enemy airfields. Activation of the system during aircraft takeoff would be accomplished by an acoustic sensor. Upon receipt of the proper acoustic signature, the missile would pop-up, acquire the target with infrared techniques, and home on and destroy the target. Target acquisition would be accomplished by a linear IR detector array, and terminal homing would be provided by a Redeye-type seeker head.

In addition to the airfield-denial application, the SIAM concept provides a possible submarine defense against ASW forces. This concept calls for the missile to be launched from a submerged submarine, deployed on the ocean surface, and fired against Soviet ASW helicopters. Activation of the system would again be accomplished by acoustic signal, and IR acquisition and terminal homing systems would again be employed.

One of the key items in the successful operation of these systems is the infrared acquisition system. This report presents an analysis of such a system for both the airfield denial task and the submarine defense task.

Study Parameters

The acquisition system comprises a linear detector array and an optical system having a fan-shaped field-of-view of 64 by 0.11 degrees. Scanning is accomplished by rotation of the missile about its spin axis. Acquisition probabilities are

governed by the signal-to-noise ratio in the detector channels. In this analysis, the spectral radiant intensities of an F-4B Phantom II and a CH-47C helicopter and typical MIG 21 aircraft maneuvers were used to characterize the targets. The LOWTR 1 2 computer code obtained from AFCRL has been used to compute atmospheric transmission. Background spectral data in the 1.5 to 5.4 μ regime were utilized. Target range and aspect angle were obtained from a separate engagement analysis[2] for five different aircraft maneuvers and two different helicopter locations.

In the airfield denial task, five possible maneuvers are considered for the MIG 21 aircraft. They are nominal, low slow, low fast, spiral, and maximum climb.[2] The first two maneuvers involve operation at military power and cruise power, respectively. The last three maneuvers are performed under full afterburner conditions. The missile system usually operates in the tail-chase mode so that a favorable aspect angle is obtained. However, in the submarine defense task, this situation is not always realized, and lower target intensities and shorter acquisition ranges are to be expected.

System Description

The SIAM concept for the airfield denial task is illustrated in Figure 1. Details of system operation are given in References 1 and 2. The remotely implanted missile is activated upon receipt of an acoustic signal from a departing aircraft. After a delay to allow for cooling of the infrared sensors, the missile pops up, acquires the target with an infrared detection system, and turns in the direction of the target. At the proper point in the missile trajectory, guidance is handed over from the acquisition system to the terminal homing system. Present plans envision the use of a Stinger (improved Redeye) tracking head for terminal phase guidance.

Deployment of a similar missile system for submarine defense is illustrated in Figure 2. Here, the missile is launched through the signal ejection port of the submarine. It remains on the ocean surface in a flotation mode until the receipt of an acoustic signal from the ASW helicopter. After launch, the operation of the missile is similar to that in the airfield denial task.

Key factors influencing successful infrared acquisition system operation are the optical system, the detection system, and target and background characteristics.

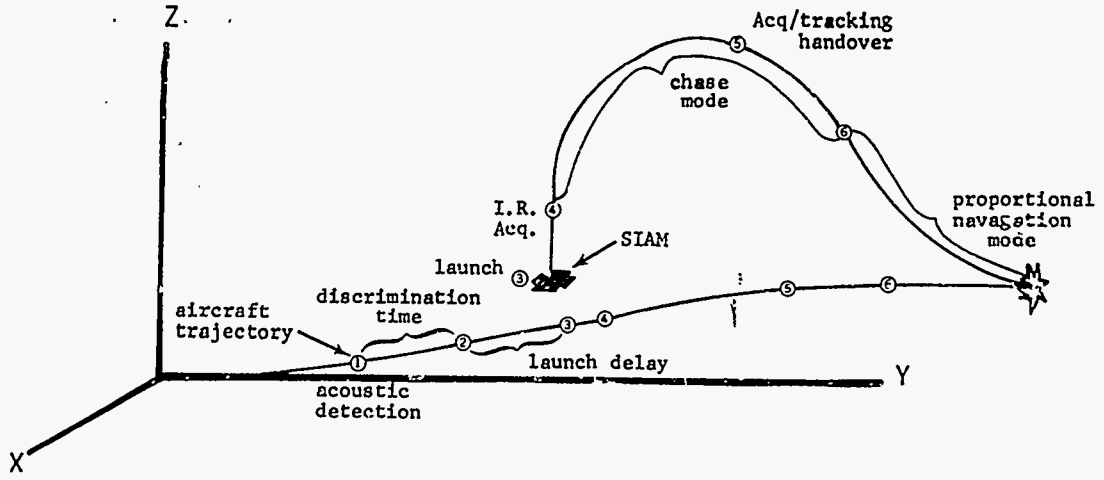

Figure 1. Illustration of airfield denial task

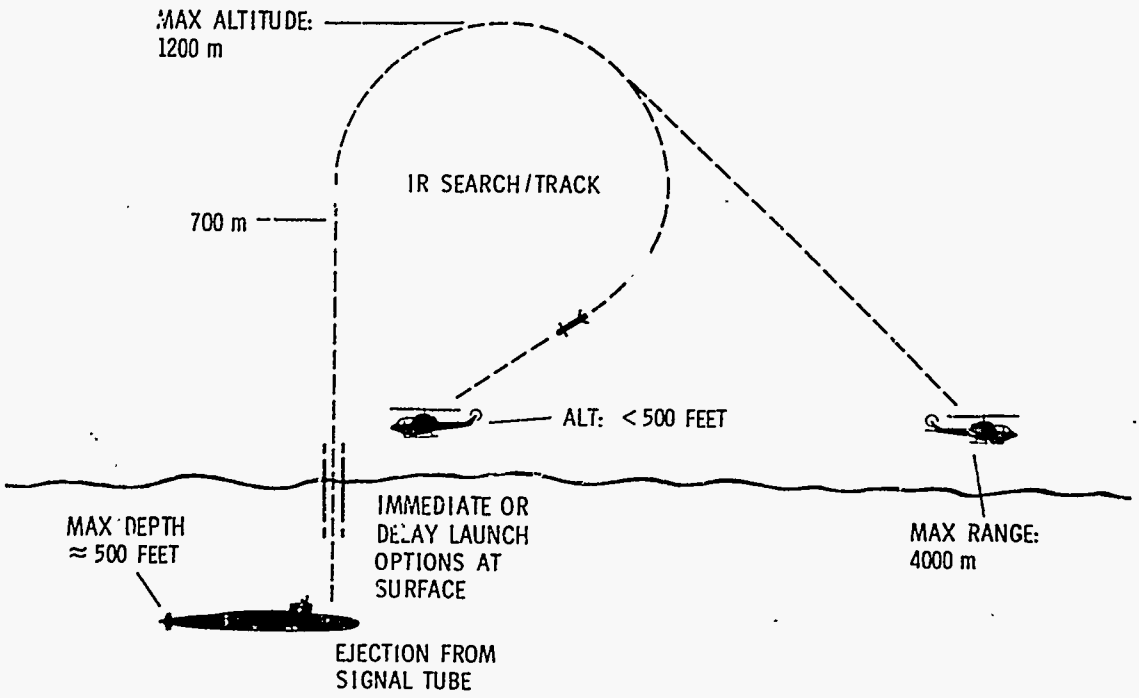

Figure 2. Illustration of submarine defense task

Optical System

Search and acquisition are accomplished with a linear detector array and an optical system whose field-of-view sweeps out a region of space as the missile rotates about its spin axis. The situation is depicted in Figure 3. Two optical systems, each having a fan-shaped field-of-view of 32 by 0.11 degrees, are used to provide a total coverage of 64 by 0.11 degrees. An array of small detector elements

provides a small field-of-view for each elemental detector; as will be seen later, this is important in reducing the deleterious effects of background clutter. In the system considered here, the elemental field-of-view is 2 by 0.11 degrees. A folded Schmidt optical system will be used to minimize space requirements. Present design provides an f/1.0 optical system.

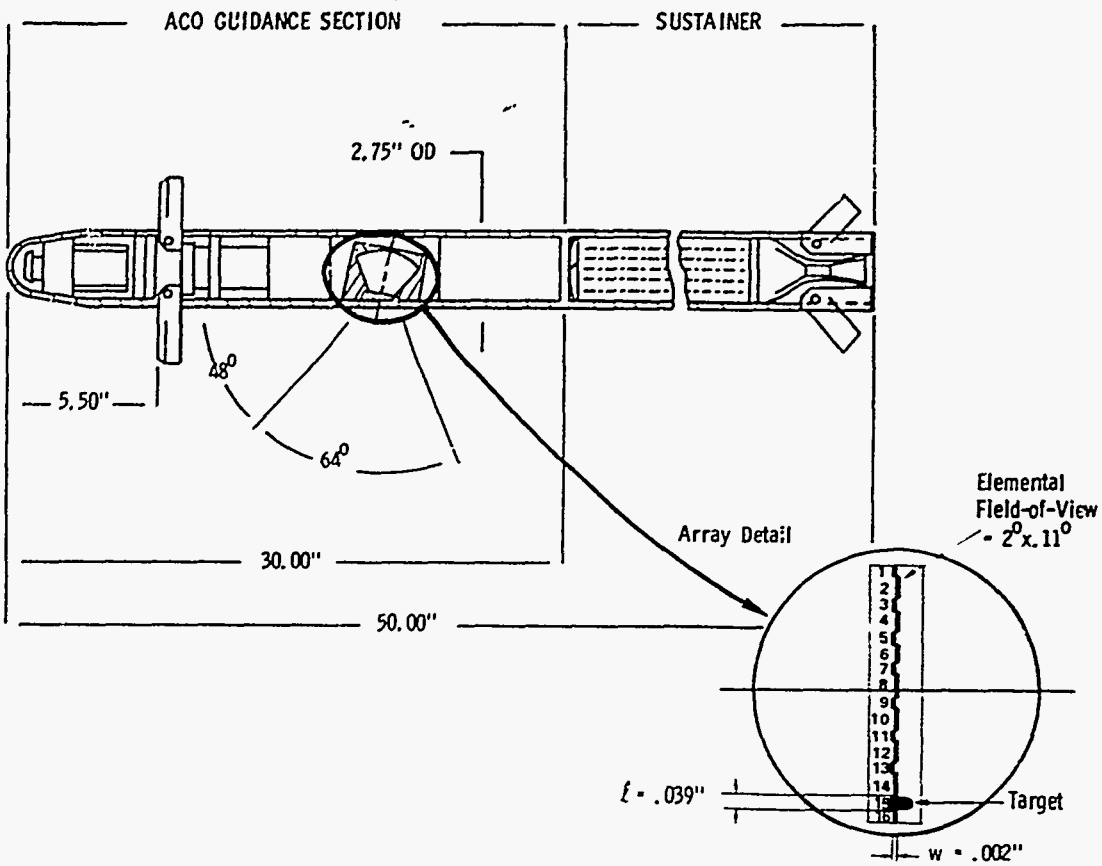

Figure 3. Optical system

Detection System

The performance of the acquisition system is described in terms of the probability of detecting a target under certain given conditions. This probability depends critically on the signal-to-noise ratio (S/N) at the output of the infrared photodetector. The fundamental equations describing the performance of the SIAM acquisition system are given in Appendix A. The S/N is specified in Eq. (A-11) as a function of the characteristics of the target, the background against which the target must be detected, the intervening atmosphere, and the sensors themselves.

As the missile spins, the signal from each elemental detector will fluctuate as its field-of-view encompasses varying amounts of background and target radiance. A hypothetical single-scan variation is indicated in Figure 4. Sensor performance is determined by the contrast between the minimum signal generated when the target is present and the maximum signal generated by the background clutter. Threshold detection is a commonly used technique for detecting such contrasts. However, because the background radiance level varies in time through wide values relative to the detector noise level, the threshold level cannot be clamped at an absolute value. It must practically be referenced to the average background radiance received during some previous time period. With this technique system operation is limited by the amount, in relation to the noise equivalent flux density of the detector, by which the target-generated signal exceeds the background contrast.[3]

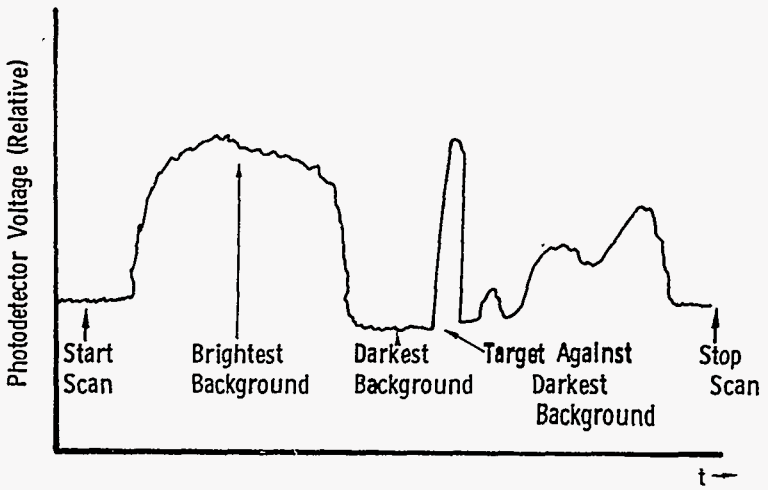

Figure 4. Hypothetical variation of detector voltage with time for a single scan

Equation (A-11) includes a factor, D, called the background discrimination factor. This factor can be used to describe the effectiveness of background discrimination techniques. A value of unity for D can be obtained with the detection scheme illustrated in Figure 5. Here an automatic gain control (AGC) system with the proper time constant is used to reduce the effects of background clutter. The AGC circuit must average the slowly varying component of the background radiance while passing the faster target pulse. Should completely effective background discrimination techniques be possible (or no background clutter be present) the value of D may be reduced to zero. Detection probabilities for both cases will be discussed later.

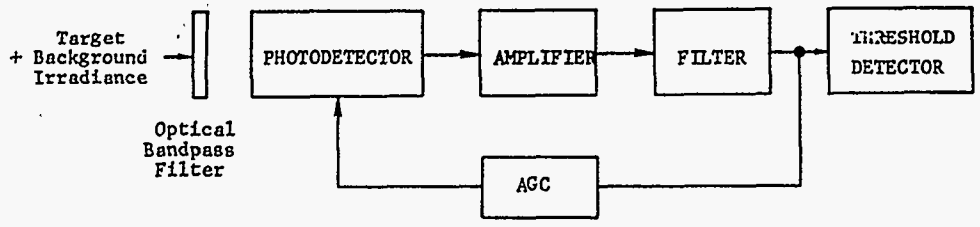

Figure 5. Block diagram of AGC detection scheme

Target Radiation Characteristics

Evaluation of the S/N requires specification of the radiant intensity of the target. In this report, two possible targets are considered. For the airfield denial task, the MIG 21 aircraft is a representative target[1] and for the submarine defense task the Hormone-class ASW helicopters of the Soviet Union are representative targets.

Spectral distributions of radiant intensity are required for both targets. Extensive intensity measurements have been made on U. S. aircraft;[4,5] unfortunately, little spectral data are available on the Soviet counterparts. Consequently, the IR spectral signatures of the F-4B Phantom II aircraft and the CH-47C helicopter have been used in this report for S/N evaluation. Spectral radiant intensity curves for both are shown in Figure 6. Maximum intensity is observed in the 2.5 to 5.0 μ wavelength interval. These curves are smoothed versions of the raw data appearing in References 4 and 5. The minima at 2.7 and 4.3 μ result from absorption of radiation by atmospheric water vapor and carbon dioxide, respectively. Both curves were obtained at tail aspect and at short ranges from the target. Because of the nature of the radiation mechanism (hot metal or plume), little difference should be noted in the emission spectra for Soviet aircraft.

In addition to specifying the spectral distribution of the target intensity, the variation of intensity with aspect angle must also be known. At the rear aspect, blackbody radiation from hot metal parts plays a dominant role; whereas, at nose and side aspect, the emission produced by the hot exhaust plume becomes important.[4] Plume effects are pronounced in the 4.15 to 4.2 μ and 4.4 to 4.5 μ wavelength intervals. Variation of radiant intensity with aspect angle for the MIG 21 aircraft is shown in Figure 7 taken from Reference 6. Intensities in the 3.9 to 5.2 μ wavelength interval are given. Values are given for cruise power, military power, and maximum afterburner throttle settings. The spectral curves of Figure 6 are adjusted to agree with the intensities shown in Figure 7 over the wavelength interval 3.9 to 5.2 μ prior to performing the S/N computation.

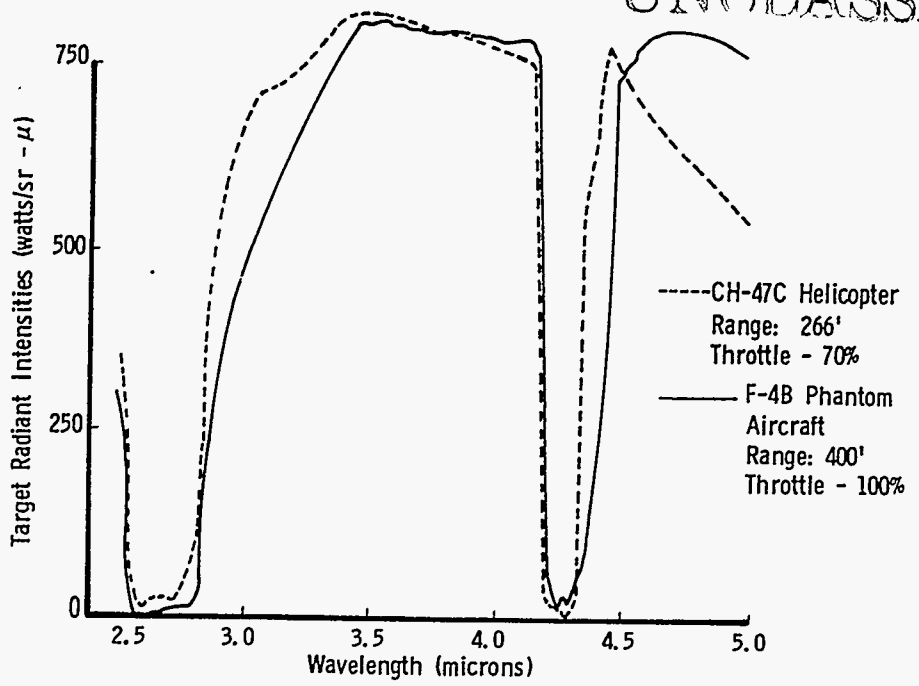

Figure 6. Curve of target radiant intensities--tail aspect--for F-4B and CH-47C

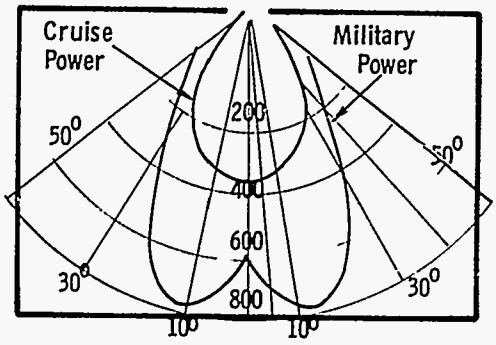

a. At cruise and military power

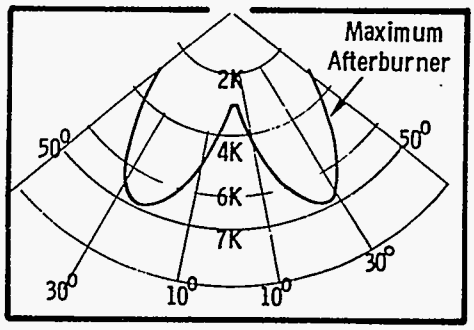

b. At afterburner power

Figure 7. Aspect function for MIG 21

Necessary aspect function data for the Soviet Hormone helicopters are not available to the author's knowledge. Consequently, the function shown in Figure 8 was synthesized from Reference 5. Engine placement on Hormone helicopters is on top of the fuselage. Therefore, the best viewing for IR detection is from the top and rear.

The data in Figures 6, 7, and 8 are used in evaluating the S/N.

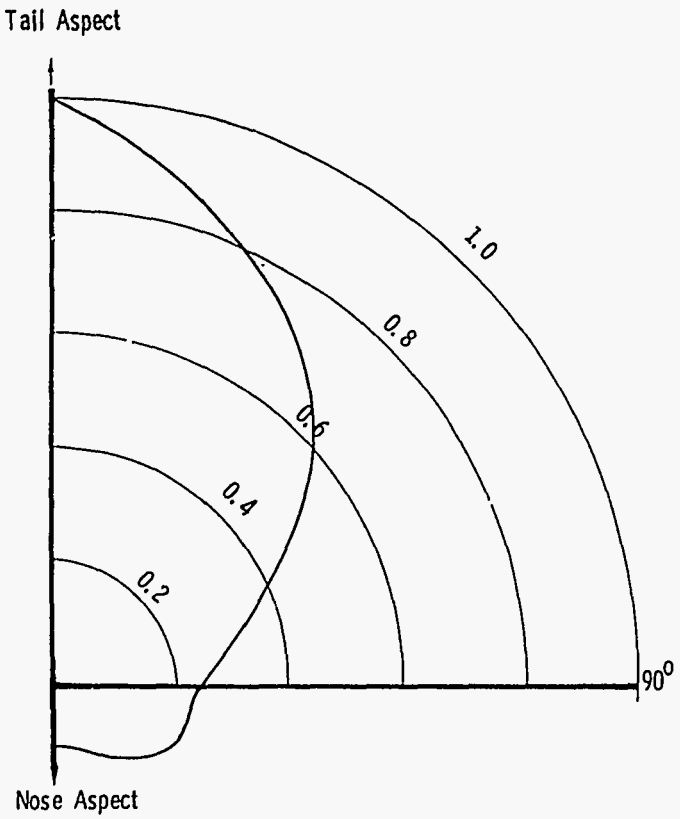

Figure 8.

Synthesized aspect function for helicopter radiance

Atmospheric Transmission

Atmospheric transmission of infrared radiation decreases with distance through the atmosphere. Absorption lines resulting from various atmospheric molecules are located throughout the IR spectral region. The spectral bandpass of the acquisition system should be selected to avoid these lines. Computations of transmission as a function of wavelength are performed in this analysis by the LOWTRAN 2 computer code.[7] This code predicts the transmittance of the atmosphere between any two specified points in the spectral region 0.25 to 28.5 μ. The spectral resolution is 20 cm^{-1}. The program provides a choice of six atmospheric models and two haze models. Molecular absorption, molecular scattering, and aerosol extinction are considered. Data

may be at wave number intervals of 5.0 cm^{-1}. The U. S. Standard Atmosphere with visibility of 23 km has been chosen for the calculations presented in this report. Figure 9 is an example of the atmospheric transmittance in the wavelength region of interest obtained from LOWTRAN 2 code. The effect of a decreased visibility (5 km) is also shown for comparison. For this example, two points separated by a slant range of 3.2 km and located at altitudes of 0.326 km and 1.095 km were chosen.

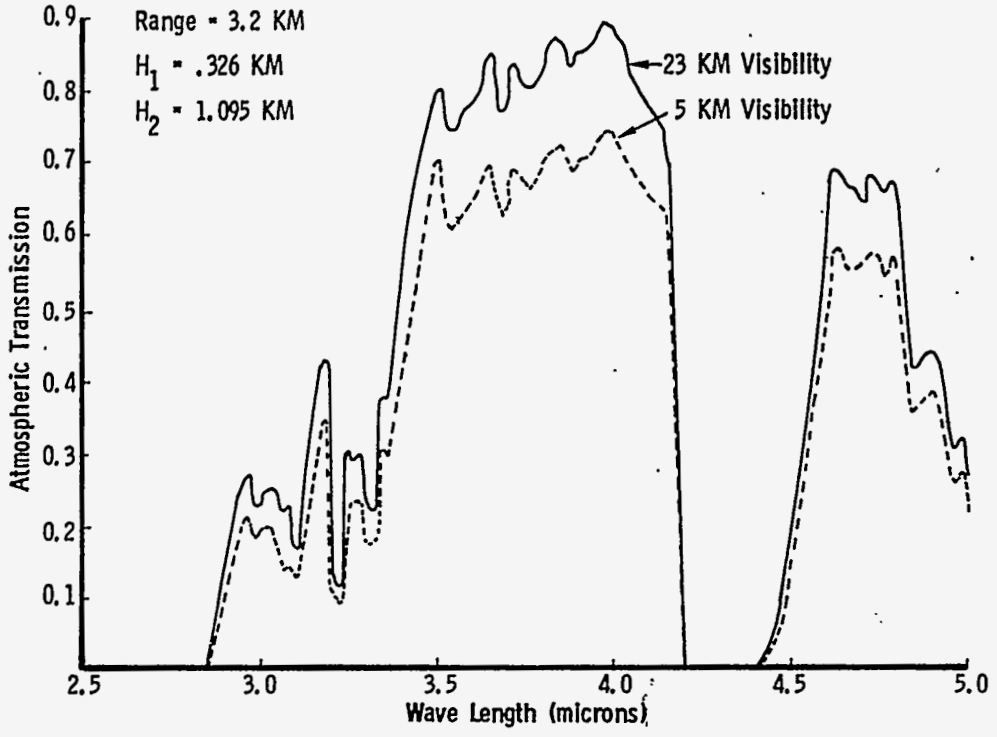

Figure 9. Atmospheric transmission as a function of wavelength

The effects of fog and clouds on system performance are not addressed in this report. It is well known[8-10] that the presence of these elements severely reduces the atmospheric transmission at infrared wavelengths.

Background Models

Background clutter is the most severe impediment to the successful operation of the SIAM system. Target acquisition must occur in most cases at a relatively low target altitude where ground clutter can be severe. To assess the effects of this clutter on system performance, background radiance as a function of wavelength must be specified in Eq. (A-11), Appendix A. Fortunately, a large body of background data has

been compiled.[11] An example of these data is shown in Figure 10. Background radiances of a blue sky and of a cloud are shown in Figures 10a and 10b, respectively. Of primary interest in the evaluation of the system S/N is the value of the background contra t as specified in Figure 10c.

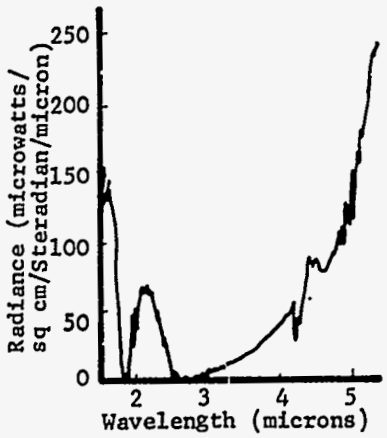

a. Spectral radiance of blue sky

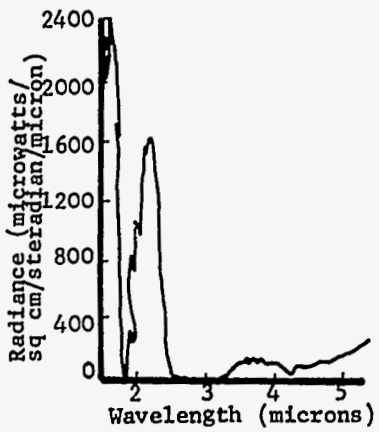

b. Spectral radiance of a cloud

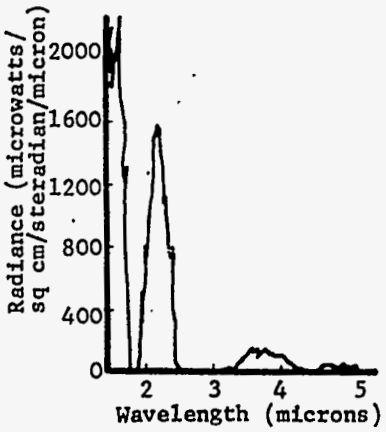

c. Blue sky/cloud contrast radiance

Figure 10.

Reference 11 provides background radiance values for 15 different background contrast situations. These curves have been digitized and used in the computer simulation of system performance. Assignment of unity value to the discrimination factor D in Eq. (A-11), Appendix A, corresponds to the conservative assumption that the background radiance changes from a minimum value (N_λ(min)) to a maximum value (N_λ(max)) in scanning a single detector width, i.e., the background clutter has very sharp edges. The effective value of [N_λ(max) - N_λ(min)] in the S/N equation may in practice be lower than the values indicated in the contrast curves in Reference 11. This stems from the fact that these are "d-c" contrast values, obtained, for example, from measurements at the center of a cloud and of a patch of blue sky. Actually the effective value of the contrast may decrease greatly as the field-of-view of the detectors is decreased because higher spatial background frequencies are utilized. While not enough data are available for firm conclusions, it appears[12] that the background radiant power falls off as the reciprocal of the spatial frequency raised to some power. The exponent varies between 1.5 and 4. In the present calculations of system performance, the d-c values of background contrast are assumed, and the estimates thus obtained should prove to be conservative.

Detection Probability Requirements

The equations describing the detection probability for an infrared acquisition system are given in Appendix B. Detection probability depends critically upon the S/N ratio at the photodetector output and upon the false alarm probability requirements. In this report, a false alarm probability of 10^{-6} was assumed. This probability implies a time of 64 seconds between false alarms caused by noise spikes. The missile flight time is of the order of 20 seconds. For this false alarm probability, a signal-to-noise ratio of 7.0 (16.9 dB) gives a single look detection probability of 0.98.

System Performance

Acquisition capabilities of the infrared system previously described have been assessed for both the airfield denial task and the submarine defense task. In both cases, data on likely missile and target trajectories were obtained from Bennett.[2] S/N values were computed throughout the launch-to-intercept trajectories. Particular emphasis was placed upon the S/N at a time of 1.1 seconds after interceptor launch,

the time at which target acquisition is assumed in Bennett's calculations. The first step in evaluating the S/N is parameter specification.

Sensor Parameters

The fixed parameters chosen (Eq. (A-11), Appendix A) for the initial design are as follows:

$A_c = 5.06\ cm^2$ = collecting area of the optical system.

$A_d = 5.03 \times 10^{-4}\ cm^2$ = area of elemental detector.

$\Delta f = 1.57 \times 10^4$ Hz = bandwidth of the electrical filter.

$\omega = 7.79 \times 10^{-5}$ sr = field-of-view of elemental detector.

$T_o = 0.9$ = transmission of optical system.

Other system parameters which are at the control of the designer are the detectivity[13] of the photodetector, D^*_λ; the transmission characteristics of the optical filter; and the area correction term η. Other parameters needed in evaluating this equation are determined by factors outside the designer's control.

The sensor detectivity, D^*_λ, characterizes the noise voltage generated by the photodetector. It is a property of the material chosen for use as the photosensor. Original calculations were performed with InSb which has a peak D^*_λ of approximately 10^{11} $[cm(Hz)^{1/2}]$/watt at a wavelength of 5 microns.[14] However, this material prefers to operate at a temperature of 77°K, and initial estimates of the cooling capability of an acceptably sized dewar indicated that there might not be sufficient time between system activation and launch to cool the detectors to this temperature. Discussions with detector manufacturers indicate that certain proprietary processes can yield adequate detectivities in the material ((Hg, Cd), Te) at a more acceptable temperature of 200°K. Consequently, the curve shown in Figure 11 was used for D^*_λ in this analysis.

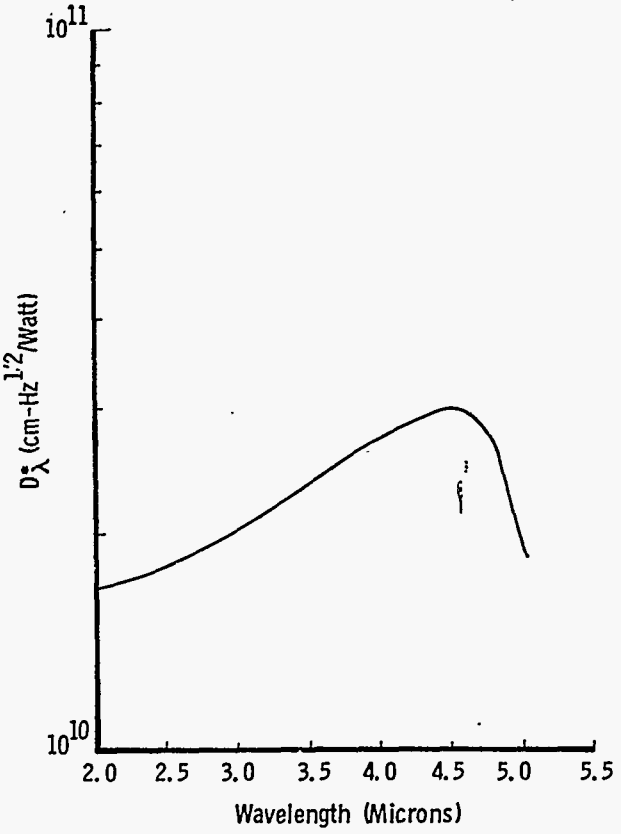

Figure 11. D^* as a function of wavelength for ((Hg, Cd), Te) at 200°K

Spectral Bandpass Selection

Maximization of S/N of the acquisition system involves maximizing the contribution to the signal from the target while minimizing the contribution from the background. Variation of the spectral bandpass of the optical filter preceding the detectors affects both of these quantities. Manufacturers of infrared track-while-scan sensors have used different wavelength bands for different applications. For example, Aerojet-General Corporation has designed and built a system operating at 2.85 to 3.19 μ for the B-1 aircraft;[15] AVCO Corporation has built a tail warning device for use on the F-111 aircraft which operates in the 3.8 to 5.5 μ wavelength region;[16] and Hughes aircraft has designed three different systems for possible use on the AWACS, B-1A, and F-111D aircraft which operate in the plume-sensitive 4.1 to 4.7 μ regime.[17] An inspection of Figure 6 reveals that the peak radiant intensity from the target occurs in the 3.0 to 5.0 μ wavelength band for small aspect angles.

Atmospheric transmission is also high in this band as evidenced in Figure 9. These factors indicate that an optical filter located within the 2.5 to 5.0 μ band is the best choice for maximizing the signal received from the target.

Consideration must also be given to the spectral distribution of the background radiance. Spectral contrast radiance for a blue sky/cloud situation has been illustrated in Figure 10c. In general, the shape of the spectral radiance curves is different for different backgrounds, although the absolute radiance levels are generally always less than 120 microwatts/cm^2-sr-μ in the spectral region 2.5 to 5 μ. Figure 12, obtained from data in Reference 11, illustrates this trend. Here, cloud radiance is seen to peak near 3.6 μ, while radiance from the ocean and sky have their highest values near 5.0 μ. These facts indicate that it might not be possible to pick one single spectral bandpass within the 2.5 to 5.0 μ regime which would yield an adequate value of S/N ratio for all possible backgrounds, i.e., a filter yielding optimum S/N for a cloud background might yield a suboptimum value for the blue sky or ocean background. Background radiance levels are high enough in several cases to cause the S/N to take on negative values. This means simply that the background contrast irradiance at the sensor exceeds that received from the target. In this case, the AGC system alone is not sufficient for target detection.

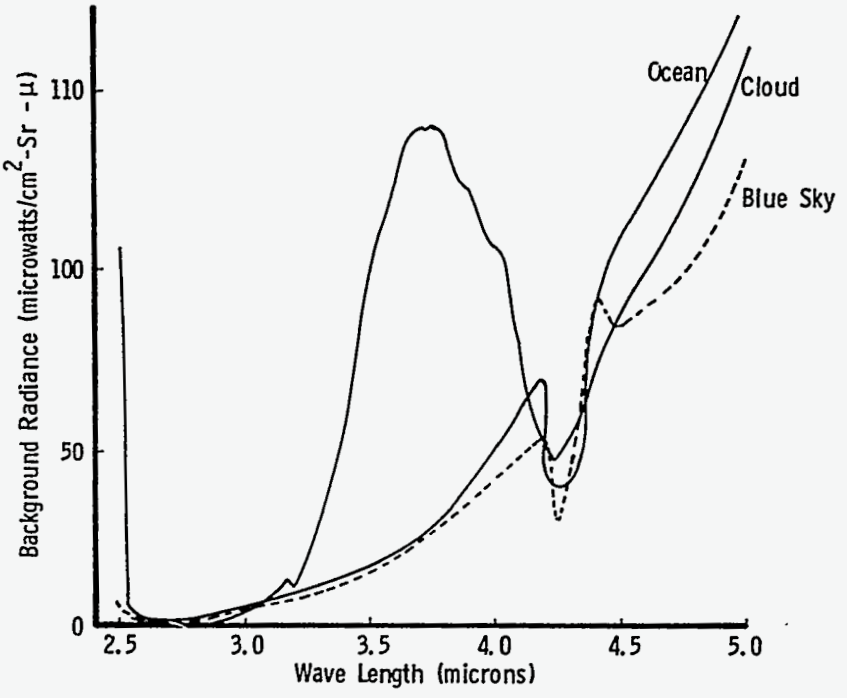

Figure 12. Background spectral radiance for cloud, ocean, sky

Table I lists values of S/N for two different spectral filter bandwidths for all backgrounds considered. These data are for one of the trajectories in the airfield denial task. A full explanation of the different trajectories will be given later. The table lists S/N for D = 0 (perfect discrimination or uniform background) and for D = 1 (AGC system, no other discrimination) and illustrates the variation in S/N for fixed spectral bandpass as different background levels are encountered. For this particular trajectory, the spectral bandpass $4.15\ \mu \leq \lambda \leq 4.60\ \mu$ (favorable to plume radiation) gives a higher percentage of positive S/N values than does the $3.38\ \mu \leq \lambda \leq 4.17\ \mu$ bandpass filter. Note, however, that all the S/N values except the D = 0, $3.38\ \mu \leq \lambda \leq 4.17\ \mu$, case yield S/N values which are too low for adequate detection probability for this trajectory. In general, the negative values of S/N obtained with the 3.38 to 4.17 μ filter are larger in magnitude than those obtained with the 4.15 to 4.6 μ filter. This means simply that the signal generated by scanning a background scene with sharp edges will have a greater transcendence over the target signal in the former case than in the latter. At first glance, this seems undesirable. However, consideration of the D = 0 values indicates that the target signal, relative to the detector noise, is higher in the former case. The proper choice of spectral bandpass must then depend upon the signal processing logic employed. For example, the purpose of an AGC system is to drive the detector output to the detector noise level in some given time after encountering the background. If the target appears sufficiently far from the edge of the background so that the detector output has been set near the noise limit, the 3.38 to 4.17 μ interval should be chosen. If, however, the target appears near the edge of the background, i.e., within one AGC time constant, the target will more likely not be seen if the 3.38 to 4.17 μ filter is used. These arguments are predicated on the assumption of sharp background edges. Experiments involving actual backgrounds must be conducted to determine the severity of the edge problem. These data can be used in selecting AGC system time response and the optimum optical filter.

In general, the best possible discrimination techniques should be employed so that the system bandpass can be increased to permit utilization of the entire target spectrum. Table II illustrates this point. Here, the same trajectory is utilized, a cloud/sky background is assumed, and system performance for nine different spectral bandpasses is illustrated. Positive values are indicated for D = 1 for only two of the spectral intervals. Again, the positive values, when obtained, are low. Better results are obtained when good discrimination techniques are employed and the spectral bandpasses are increased.

TABLE I

S/N Values for Different Backgrounds
(One Point in Nominal Trajectory)

Curve Number in Ref. 13	Background	S/N			
		3.38 μ ≤ λ ≤ 4.17 μ		4.15 μ ≤ λ ≤ 4.60 μ	
		D = 0	D = 1	D = 0	D = 1
1C	Blue sky/mountain snow	7.26	- 25.6	2.42	1.15
2C	Snow/sky	7.26	- 35.2	2.42	- 1.24
3C	Blue sky/cloud	7.26	-137.4	2.42	- 5.22
4C	Sky/cloud	7.26	-143.6	2.42	- 5.13
5C	Blue sky/mountain peak	7.26	- 82.9	2.42	-26.9
6C	Blue sky/tree	7.26	- 11.6	2.42	- 1.30
7C	Snow/shaded ground	7.26	- 4.9	2.42	- 6.66
8C	Blue sky/snow covered mountain	7.26	- 3.1	2.42	0.12
9C	White surf/cliff	7.26	4.0	2.42	0.36
10C	Sky horizon/ocean horizon	7.26	- 5.4	2.42	2.00
11C	Sky/land strip	7.26	4.0	2.42	1.73
13C	Sky/ocean (1)	7.26	- 28.9	2.42	1.97
14C	Sky/ocean (2)	7.26	-322.0	2.42	1.71
15C	Mountain/sky	7.26	1.9	2.42	1.74
18C	Land/ocean	7.26	1.5	2.42	2.34

TABLE II

S/N for Cloud/Sky Background
(One Point in Nominal Maneuver)

Spectral Interval (μ)	S/N	
	D = 0	D = 1
2.5 to 3.3	0.4	- 4.4
2.84 to 3.18	0.3	- 1.4
3.38 to 4.64	9.3	-148.0
4.15 to 4.25	1.2	- 5.4
4.4 to 4.55	0.8	0.7
4.42 to 4.64	1.6	0.2
2.5 to 5.0	12.64	-177.4
4.4 to 5.0	4.35	- 21.2
3.0 to 5.0	12.57	-176.3

In summary, the proper choice of spectral bandpass depends to some extent upon the discrimination techniques employed. While the data shown in Tables I and II are for one of the worse-case trajectories, it is evident that successful system operation demands good discrimination against background clutter. If near perfect (D = 0) discrimination can be employed, the spectral bandpass from 3.0 to 5.0 μ can be utilized to yield adequate S/N values. Discrimination techniques will be discussed in a later section of this report. However, if the elemental field-of-view ω were reduced by a factor of 3, the effects of background clutter could be virtually eliminated, if all other system parameters remained fixed. Unfortunately, this would require smaller detector elements which appears to be beyond the present state-of-the-art in detector fabrication.

Acquisition Capabilities for the Airfield Denial Task:

Bennett[2] has evaluated SIAM missile performance against five possible maneuvers for the MIG 21 aircraft. From these hypothetical maneuvers and a knowledge of the capabilities of the acoustic sensor system, emplacement footprints about the airfield were derived. Missiles implanted within these footprint areas have miss distances of from 0 to 6 meters when it is assumed that the target is acquired at a time of 1.1 seconds after launch.

A grid showing the emplacement arrangement in relation to the runway is shown in Figure 13. Acquisition probabilities were computed for missiles fired from each point in the implantation grid for each of five assumed target takeoff maneuvers as follows:

1. Nominal -- aircraft takes off with full afterburner, climbs to 50 feet altitude, accelerates to 550 ft/sec, cuts afterburner, and climbs out on military power at 15 degrees.

2. Maximum Climb -- aircraft takes off and climbs out at 33 degrees at full afterburner.

3. Low Fast -- aircraft takes off with full afterburner, climbs to 70 feet altitude, and flies out at this altitude at full afterburner.

4. Low Slow -- aircraft takes off at full afterburner, climbs to 50 feet, cuts afterburner, and flies out at 50 feet altitude at cruise power.

5. Spiral -- aircraft takes off with full afterburner, initiates a 2 g lateral turn, and climbs at maximum rate to make axial acceleration zero with full afterburner.

The above maneuvers are illustrated in Figure 14. Acquisition capabilities for each of these maneuvers are discussed below.

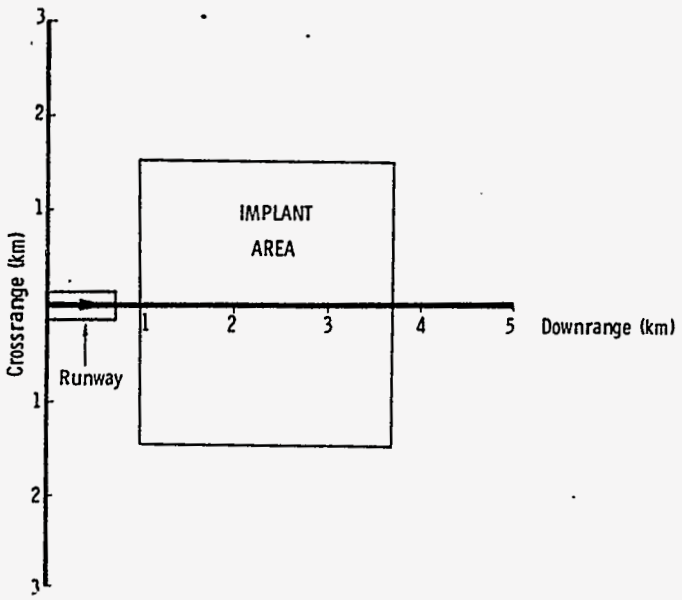

Figure 13. Footprint of implantation area for airfield denial task

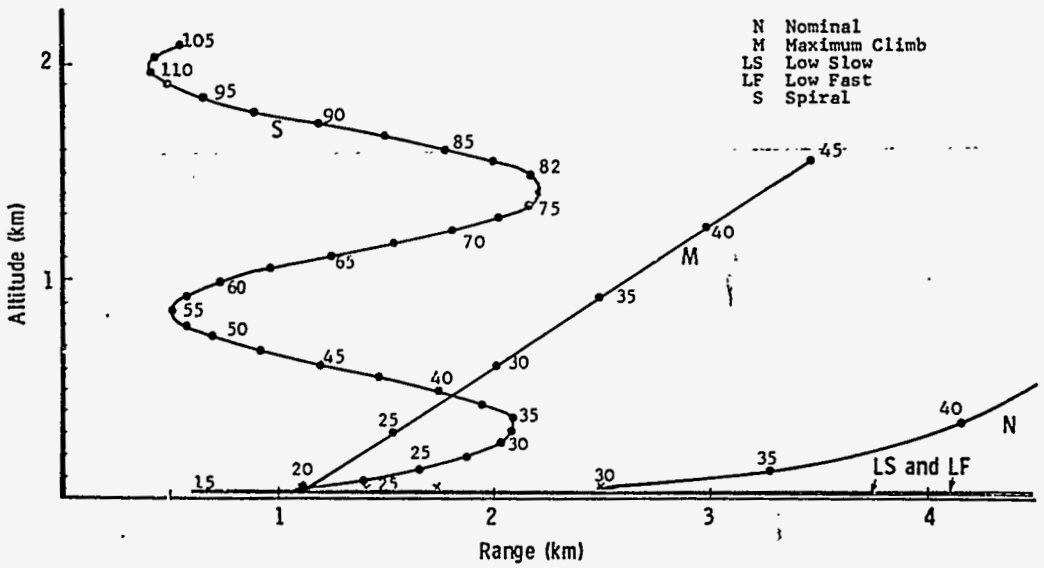

Figure 14. Aircraft maneuvers for MIG 21

Results for Nominal Maneuver -- Emplacement points for zero miss distance for the nominal trajectory are denoted by 0 in Table III. Points with miss distances greater than zero are denoted by x. Evaluation of Eq. (A-11), Appendix A, using missile and target altitudes, aspect angles, and ranges from Reference 2 on this trajectory indicates that, for perfect discrimination (D = 0), the S/N is sufficient in all cases to yield an acquisition probability of greater than 0.98 for all points in the implantation grid. The spectral bandpass of the system was fixed at 3.0 to 5.0 μ for these computations. If no discrimination other than AGC is employed (D = 1), the S/N ratio for this maneuver against a cloud/sky background becomes negative for several points. These points are denoted by asterisks in Table III. Therefore, in order to realize the kill probabilities reported by Bennett, effective discrimination techniques must be employed for the nominal trajectory. In general, a discrimination factor D = 0.3 is sufficient to yield adequate acquisition probability. Alternatively, there are some points in the footprints for which AGC-type logic is sufficient and effective P_k's may be realized by demanding more precision in missile implantation. For values of cross range in excess of 500 m, the appearance of asterisks in Table III as range increases reflects afterburner cutoff. The resulting decrease in target intensity allows the background term to dominate the S/N; therefore, effective discrimination must be employed for successful system operation.

TABLE III

Footprint for Nominal Maneuver

Cross Range (m)	Range (m)											
	1000	1250	1500	1750	2000	2250	2500	2750	3000	3250	3500	3750
1	X	X	X	0	0	0	0	0	0	0	0	0
250	X	X	0	0	0	0	0	0	0	0	0	0
500	X	X	0	0*	0*	0*	0*	0*	0*	0*	0*	0*
750	X	0	0*	0*	0*	0*	0*	0*	0*	0*	0*	0*
1000	0	0	0*	0*	0*	0*	0*	0*	0*	0*	0*	0*
1250	0	0	0*	0*	0*	0*	0*	0*	0*	0*	0*	0*
1500	0	0*	0*	0*	0*	0*	0*	0*	0*	0*	0*	0*

0 - Less than 0.5 m miss distance

X - Finite miss distance

* - Effective background discrimination must be employed

Computations of S/N as a function of time for the nominal trajectory indicate that the target is within the field-of-view of the acquisition system for a period of 2 to 3 seconds, if acquisition occurs 1.1 seconds after launch. During this time, the system must acquire the target, turn in the proper direction, and hand over tracking to the terminal system. With a spin rate of 10 rps, 20 to 30 scans are provided for acquisition.

Results for Maximum Climb Maneuver -- Table IV presents footprint data for the maximum climb trajectory. For all footprints, S/N is adequate with AGC logic because aircraft afterburner is used throughout the maneuver. The letter A denotes the positions in the footprint where the detection range of the acoustic sensor has been exceeded. 1.1 seconds after launch the aircraft is out of the field-of-view of systems launched from the positions marked with "t." If the missile is allowed to fly vertically, the target will reenter the detector field-of-view at a later time. Bennett has calculated intercept trajectories for the case of acquisition times greater than 1.1 seconds. For the maximum climb trajectory, system performance is not degraded by acquisition at times between 1.1 and 5 seconds after launch.

TABLE IV

Footprint for Maximum Climb Maneuver

Cross Range (m)	Range (m)											
	1000	1250	1500	1750	2000	2250	2500	2750	3000	3250	3500	3750
1	0	0	0-t	0-t	0-t	0-t	0-t	0-t	0-t	0-t	0-t	0-t
250	0	0	0-t	0-t	0-t	0-t	0-t	0-t	0-t	0-t	0-t	0-t
500	0	0	0	0-t	0-t	0-t	0-t	0-t	0-t	0-t	0-t	0-t
750	0	0	0	0	0-t	0-t	0-t	0-t	0-t	0-t	0-t	0-t
1000	0	0	0	0	0	0-t	0-t	0-t	0-t	0-t	0-t	0-t
1250	0	0	0	0	0	0	0	0-t	0-t	0-t	0-t	0-t
1500	0	0	0	0	0	0	0	0	A	A	A	A

A - Outside acoustic range

0 - Less than 0.5 m miss distance

t - Greater than 1.1 seconds acquisition time is required

Results for Low, Fast Maneuver -- Use of afterburner in this maneuver allows adequate probability of acquisition with AGC-type logic for all points in the implantation grid. In addition, the target is in the field-of-view for all possible implantation points. S/N values at acquisition time range from 24 to 76 dB for this maneuver.

Results for Low, Slow Maneuver -- This maneuver presents the greatest challenge to the acquisition system because the aircraft is moving under cruise power. Target radiant intensity is consequently low, and problems with background clutter are severe. The footprint for this maneuver is shown in Table V. The symbols used are as explained previously. Many of the points in the emplacement grid require effective background discrimination. For small cross range values, AGC-type logic is sufficient. However, for cross ranges greater than 250 meters, additional discrimination techniques are required. Indeed, for perfect discrimination (D = 0), the S/N is only 15 dB (P_a = 0.8) for missiles implanted at cross ranges in excess of 1250 meters. Accurate implantation is, therefore, required for successful system operation against this maneuver.

TABLE V

Footprint for Low, Slow Maneuver

Cross Range (m)	Range (m)											
	1000	1250	1500	1750	2000	2250	2500	2750	3000	3250	3500	3750
1	0	0	0	0	0	0	0	0	0	0	0	0
250	0	0	0	0	0	0	0	0	0	0	0	0
500	0*	0*	0*	0*	0*	0*	0*	0*	0*	0*	0*	0*
750	0*	0*	0*	0*	0*	0*	0*	0*	0*	0*	0*	0*
1000	0*	0*	0*	0*	0*	0*	0*	0*	0*	0*	0*	0*
1250	0*	0*	0*	0*	0*	0*	0*	0*	0*	0*	0*	0*
1500	0-M	0-M	0-M	0-M	0-M	0-M	0-M	0-M	0-M	0-M	0-M	0-M

0 - Less than 0.5 m miss distance

* - Effective background discrimination required

M - $P_d \sim 0.8$ with perfect discrimination

Results for Spiral Maneuver -- This maneuver employs full afterburner; and, as a result, acquisition probabilities with AGC logic are greater than 0.98 for most points in the implantation grid, as shown in Table VI. More points are shown here

than in the previous cases because this maneuver is asymmetric. AGC-type logic is sufficient for all points except three at 1000 m downrange. Severe aspect angle is the cause of the reduced signal intensities at these points. A few of the points at cross ranges in excess of 1000 m are unsuitable for acquisition at t = 1.1 seconds because of the view angle of the infrared system. However, the target can be acquired at a later time. Kill probabilities for this maneuver are limited more by flight dynamics and acoustic sensor capabilities than by infrared acquisition capabilities.

TABLE VI

Footprint for Spiral Maneuver

Cross Range (m)	Range (m)											
	1000	1250	1500	1750	2000	2250	2500	2750	3000	3250	3500	3750
-1500	0	0	0	0	0	X	X	A	A	A	A	A
-1250	0	0	0	0	0	0	0	X	A	A	A	A
-1000	0	0	0	0	0	0	0	0	X	A	A	A
- 750	0	0	0	0	0	0	0	0	0	X	A	A
- 500	0	0	0	0	0	0	0	0	0	0	X	A
- 250	0	0	0	0	0	0	0	0	0	0	X	A
1	0	0	0	0	0	0	0	0	0	0	0	X
250	0	0	0	0	0	0	0	0	0	0	0	X
500	0	0	0	0	0	0	0	0	0	0	0	X
750	0	X	0	0	0	0	0	0	0	0	0	X
1000	0*	X	0-t	0-t	0-t	0	0	0	0	0	0	X
1250	0*	X	0-t	0-t	0-t	0	0	0	0	0	0	X
1500	0*	X	0-t	0-t	0	0	0	0	0	0	0	X

0 - Less than 0.5 m miss distance

t - Greater than 1.1 seconds acquisition time required

X - Finite miss distance

* - Effective discrimination required

A - Outside acoustic detection range

Acquisition Capabilities for Submarine Defense Task

As described in Figure 2, the submarine defense task involves launching a missile vertically and attacking a helicopter. System activation is accomplished by an acoustic sensor as in the airfield denial task. From the standpoint of missile

dynamics, the most difficult helicopter location to attack is one at low altitude and directly above the launch point. Successful intercept of a helicopter at such a location involves having the interceptor ascend vertically to an altitude of 600 m and then to turn as sharply as possible to make the intercept. This trajectory is shown in Figure 15 (taken from Ref. 2). The numbers 7 to 18 shown in close proximity to the trajectory curve denote time in seconds after missile launch. The numbers associated with the vectors at each point indicate the angle between the missile axis and the target line-of-sight. The target is assumed to be located at an altitude of 200 m. Because of the limited field-of-view of the IR acquisition system, the target is in the field-of-view for only a short period of time during the upward trajectory (~0.5 sec). To circumvent this problem, it may be necessary to provide a memory so that the missile guidance can turn the missile in the proper direction when an altitude of 600 m is reached. Alternatively, the missile can be programmed to fly vertically in the absence of an acquisition signal until a predetermined altitude is reached. The missile could then reacquire the target as it pitches over, between 9 and 10 seconds after launch.

S/N has been computed at all points throughout this trajectory for two possible target orientations. The helicopter may be traveling away from or toward the missile as the missile turns. These are the two extremes as far as the infrared signal received from the target is concerned. Because the missile flies above the target, and the helicopter engines are located on top of the fuselage, the aspect angle problem is not severe for this scenario. S/N ratio is more than adequate for 0.98 acquisition probability using only AGC-type logic.

As the range between target and missile launch point increases, the infrared signal from the target will, of course, decrease. If the helicopter is headed toward the launch point (minimum signal case) the maximum acquisition range is approximately 4.5 km, if effective background discrimination techniques are employed. AGC-type logic is not adequate for this range for either target orientation. S/N approaches 17 dB (P_a = 0.98) for the following parameters:

D = 0
Helicopter altitude = 50 m
Missile altitude = 700 m
Horizontal range = 4.5 km
Target orientation = nose aspect

Successful operation of the SIAM missile in the submarine defense task is limited by infrared acquisition capabilities and not by missile dynamics. Maximum target acquisition range is ~4.5 km, if the effects of background clutter can be reduced.

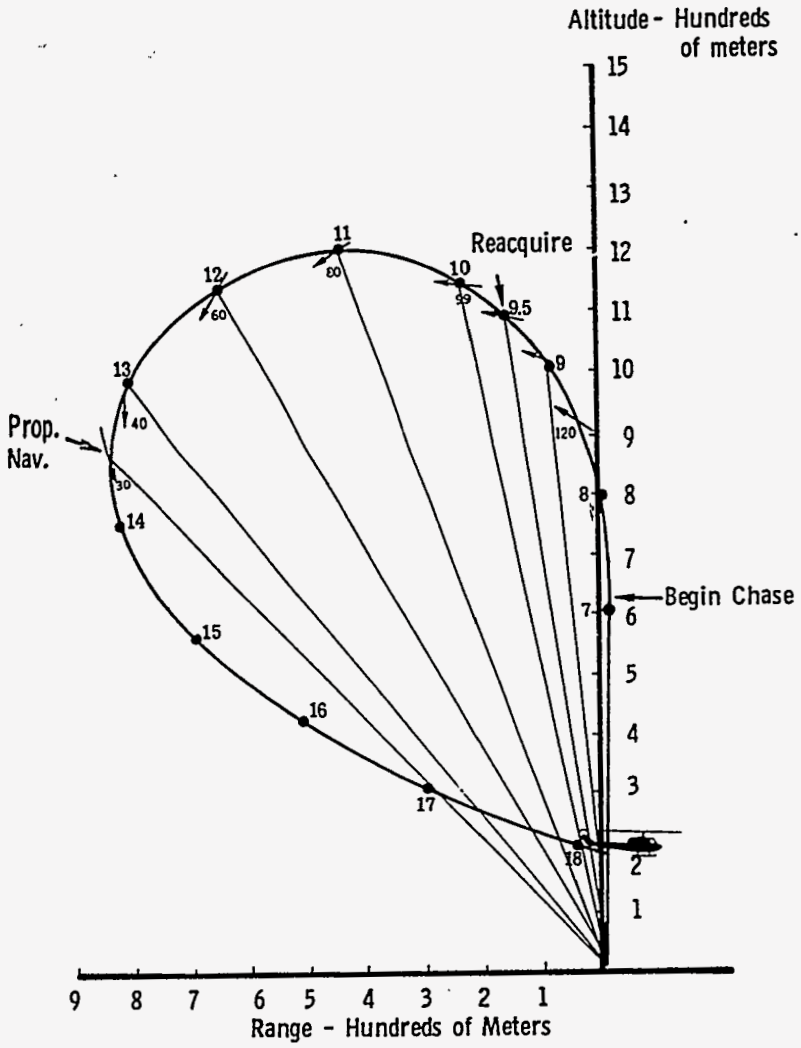

Figure 15. Interceptor trajectory -- submarine defense task

Background Discrimination Techniques

Improvements in AGC-Type System -- Ideal operation of the AGC system occurs when background clutter provides a slowly varying signal from the IR detector and the target provides a pulse of short duration. In this case, the time response of the AGC system can be adjusted to cancel the slowly varying background component and pass the signal from the target. The analysis presented here has assumed that the transition from minimum background to maximum background level is very sharp. This will probably prove to be a conservative assumption;[3] however, provision should be made for handling such a situation. Sharp background edges limit the performance of the

AGC system because the leading edge of the background pulse will be passed by the system and may cause false alarms. However, pulses from background clutter will normally be longer in duration than target pulses. Thus, to preclude false alarms, a pulse-length discrimination network may be included in the logic package. This network could be set to pass pulse lengths corresponding to a point target and yet to block the longer background pulses. A point target will be imaged onto the photodetector surface as a finite blur. The target pulse temporal characteristics depend upon the blur circle diameter and the roll rate of the missile. Blur circle diameter depends, in turn, on the characteristics of the optical system; diameters of 5.08×10^{-3} cm to 2.54×10^{-2} cm are expected. Normalized pulse shapes for different blur circle diameters are shown in Figure 16. These were computed from Eq. (C-7), Appendix C, to aid the logic system designer in specifying the proper circuitry for pulse length discrimination. A missile roll rate for 10 rps was assumed for this calculation. The pulse shape is Gaussian, produced by the Gaussian optical image of a point convolved with the scanning rectangular photodetector. For plotting purposes, all peak amplitudes were normalized to unity. This figure illustrates the direct relationship between pulse width and blur circle diameter.

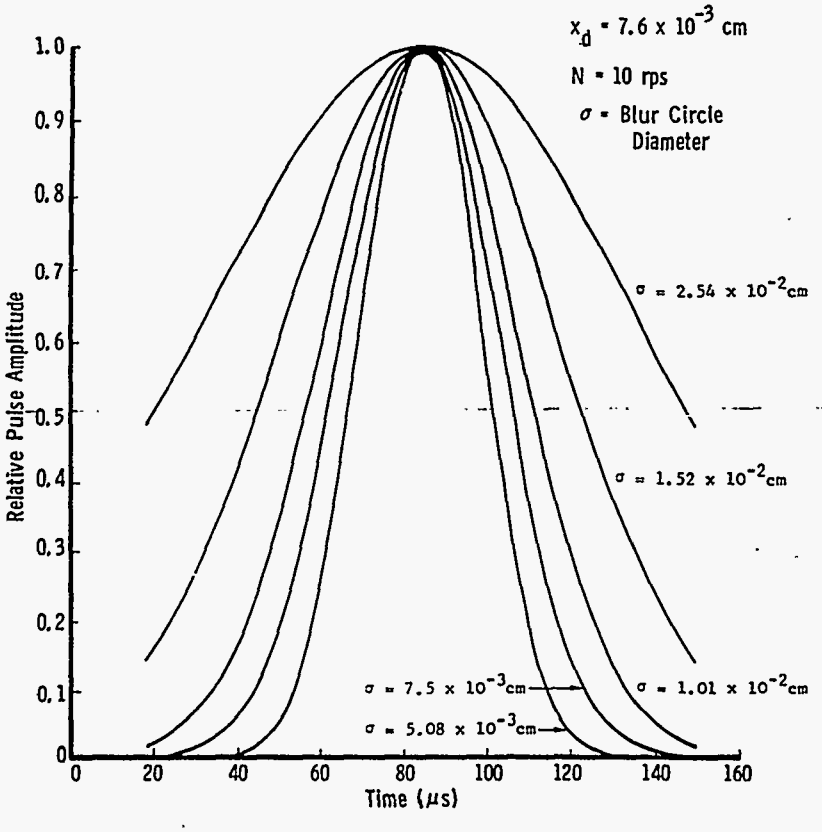

Figure 16. Normalized target pulse shapes

The pulse-length discrimination system should be designed so that pulse shapes as shown in Figure 16 generate an acquisition signal. It is expected that pulses from background clutter will look substantially different from those of Figure 16; however, more experimental data describing the sharpness of background edges are needed.

Another hindrance to ideal operation of the AGC system could arise from background fluctuations about the assumed average value. That is, the values of background radiance used in the S/N calculations reported here are the average or "d-c" values. Radiance levels can, of course, be expected to fluctuate about these average levels. If the fluctuations are rapid enough (small spatial regions) to be passed by the detection system, and have amplitudes approaching the detector noise amplitudes, reductions in S/N would be expected. The data describing spatial frequency power density of various backgrounds are, at the present time, not complete enough for a full assessment of the magnitude of this effect. However, Mundie has presented a small amount of data as shown in Figure 17 for which a sample calculation can be made. This curve illustrates the rapid decrease in background power density as the spatial frequency increases for a cloud-covered-sky background. Admittedly, these data are in a frequency band different from the one of interest here; however, the trend should carry over into the 3 to 5 μ region.

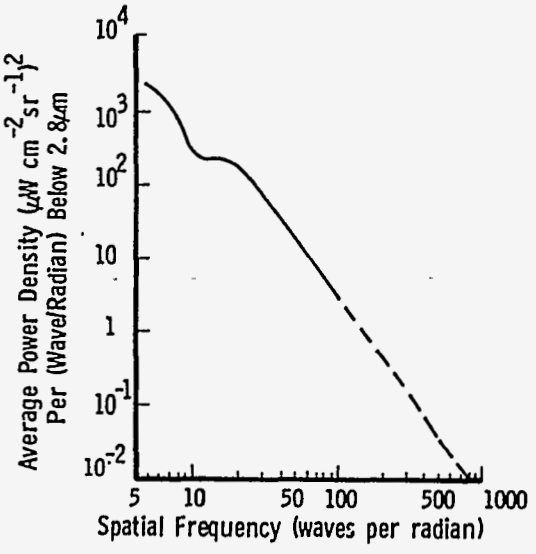

Figure 17.

Average radiant power densities for partially-cloud-covered sky background

For the sample calculation, assume a background radiance which fluctuates sinusoidally with spatial position. In a scanning system, a radiance distribution with spatial frequency k_x induces an electrical signal with frequency $k_x v$, where v is the velocity of an image point moving across the scanning detector surface.

Therefore, if f_1 is the lower cutoff frequency of the electrical network following the photodetector, the lowest spatial frequency passed by the system is given by[18]

$$k_{x1} = \frac{2\pi f_1}{v} .$$

Now $v = x_d/T_d$, where x_d is the detector width and T_d is the dwell time. For the system investigated here, v = 159 cm/sec; also, an electrical cutoff frequency of 1 kHz is assumed. With these values and an optical system focal length of 2.54 cm, k_{x1} is computed to be 100 cycles/radian. Figure 17 suggests an attenuation by a factor of 10^3 for background radiance at this spatial frequency over the "d-c" case. The electrical signal resulting from this type of background fluctuation is lower than that resulting from detector noise by a factor of approximately 10. More data are needed to properly assess this problem; however, these sample calculations indicate that the assumption of "d-c" values of background radiance in the calculations presented in this report will still yield conservative estimates of detection range.

Two-Color Discrimination -- Successful discrimination against infrared backgrounds has been accomplished through the use of the two-color technique.[19] In this technique, two photodetectors having common fields-of-view are utilized. Each detector is equipped with optical filters having different spectral bandpasses, and the outputs of the two detectors are compared to determine whether the received irradiance is from background or target. One filter is chosen to pass wavelengths which are characteristic of the target, while the other channel interrogates wavelengths where the target irradiance is low. Bandpass intervals $[\lambda_1, \lambda_2]$ for the signal channel and $[\lambda_3, \lambda_4]$ for the background channel can be chosen by the system designer. Some characteristic of the detector output, e.g., detector voltage, can be selected as the discriminant. The designer's task is then to pick the spectral intervals so that the value of the discriminant when the target is present will be substantially different from its value when only background radiance illuminates the sensor. In order to perform this selection, a computer program has been written which calculates the voltages V_1 and V_2 at the photodetector outputs for the signal and background channels, respectively, as a function of the filter bandpasses. This program was evaluated for eight of the backgrounds listed in Reference 11 for several filter bandpass intervals. The backgrounds are cloud, ocean, vegetated mountain, mountain peak, snow, sunlit snow, blue sky, and ocean below-the-horizon. In computing these values, ((HgCd), Te) with a peak detectivity of 3×10^{10} at 4.5 μ has been assumed as the detector material, and the peak responsivity of this material has been assumed to be 6×10^3 V/W. The target was assumed to be flying the nominal trajectory. The only background spectral radiance data available are in the 1.5 to 5.4 μ wavelength interval.

The first spectral interval investigated here utilized the band 4.2 to 5.0 μ for the color channel and the 3.38 to 4.17 μ interval for the signal channel. These bands are near those used successfully in Reference 19. An effective method of displaying the results of the computations is on a feature graph as shown in Figure 18. Here the voltage in the background channel, V_2, is plotted as a function of the voltage in the signal channel, V_1. In this figure, small dots represent the voltages when no target is present, and the sensor views the background indicated. When the target is present, both voltages increase to the points denoted by the larger dots. The object of this exercise is to find the optical filters which cause maximum separation between the large and small dots. A favorable case exists when a straight line can be drawn separating the target and background values. Inspection of Figure 18 indicates that this cannot be done for the postulated filter interval.

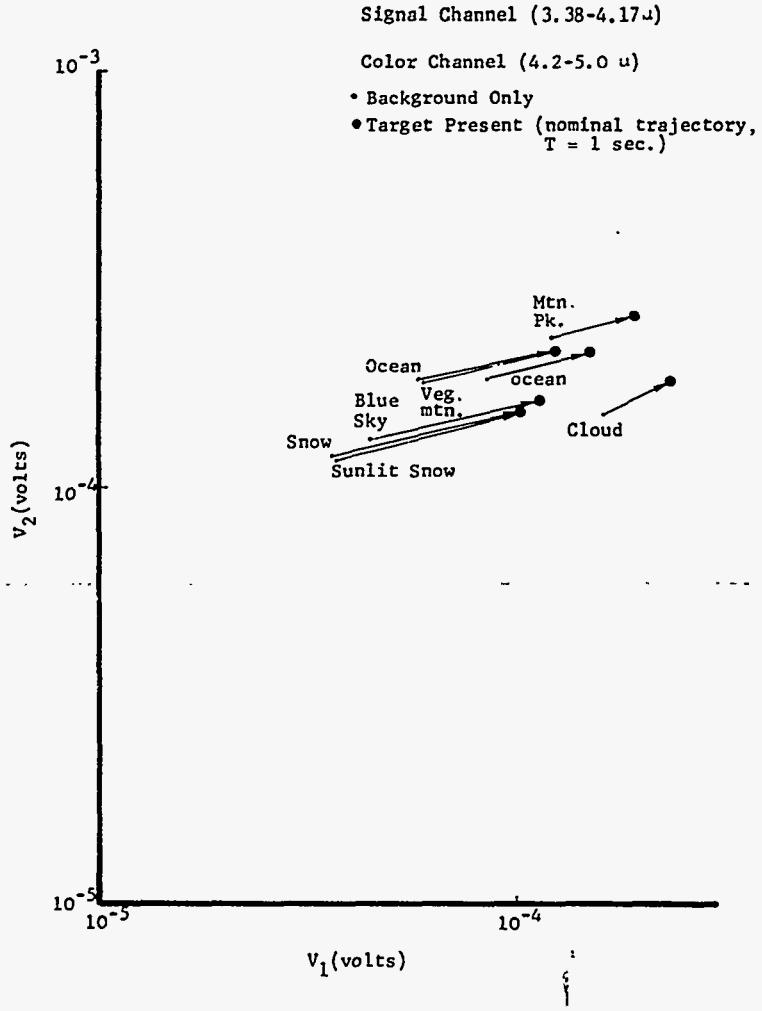

Figure 18. Feature graph for different backgrounds (color channel 4.2 to 5.0 μ, signal channel 3.38 to 4.17 μ)

Figure 19 illustrates the slight improvement which results if the signal channel bandpass is selected as 3.0 to 5.0 μ and that of the color channel as 1.5 to 2.5 μ. Here, a straight line separation can be obtained between the target and background situations, except for the mountain peak background.

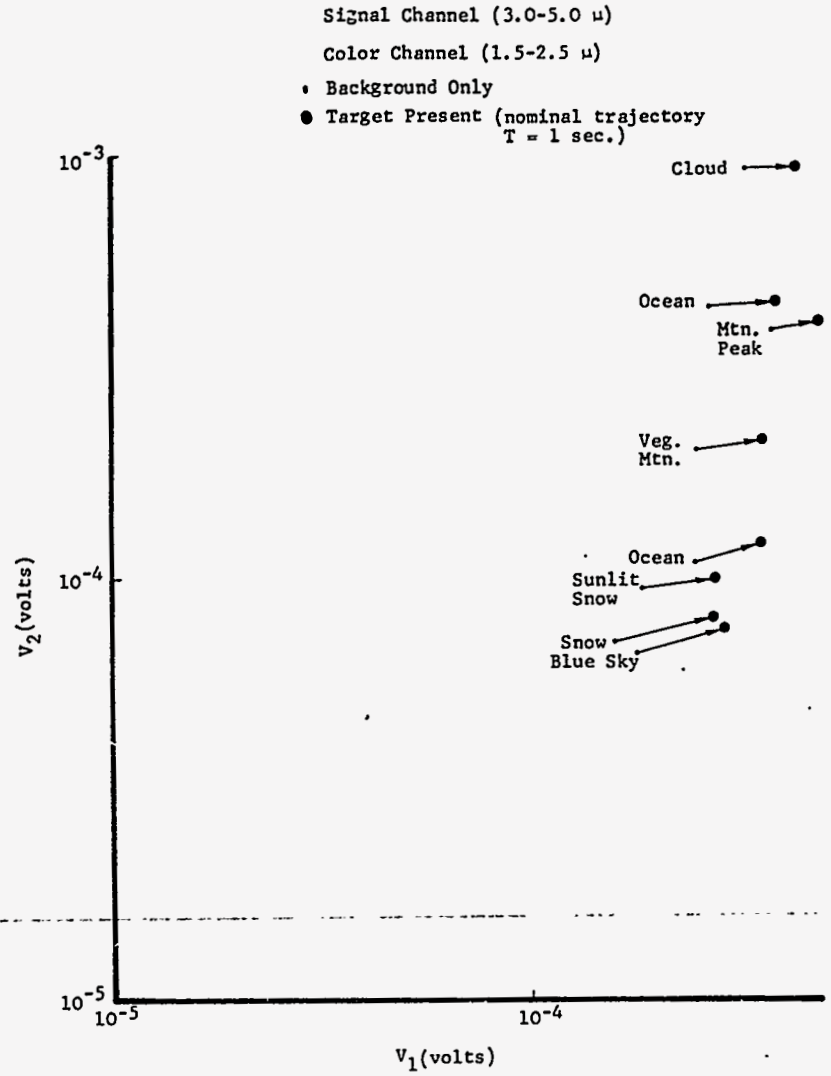

Figure 19. Feature graph for different backgrounds (color channel 1.5 to 2.5 μ, signal channel 3.0 to 5.0 μ)

Figure 20 represents the best results obtained to date in the 1.5 to 5.4 μ region. For all backgrounds considered, the target points can be separated from the background points by a single straight line. The equation of a straight line on log-log paper can be expressed in general terms as

$$V_2 = k_1 V_1^{k_2} .$$

For the line shown, k_2 has a value of 2.0. In practical terms, this finding is significant because it describes precisely the required signal processing function. The use of a simple squaring circuit in the signal channel with a variable gain amplifier (k_1) is all that is necessary to obtain proper discrimination against the backgrounds considered here.

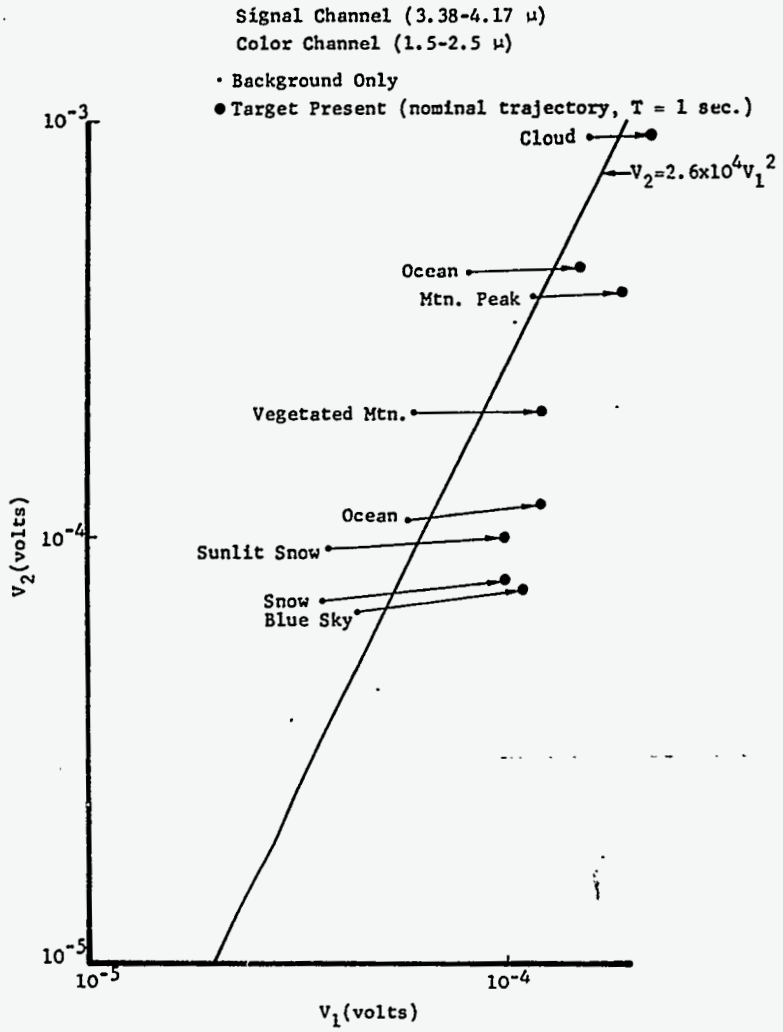

Figure 20. Feature graph for different backgrounds (color channel 1.5 to 2.5 μ, signal channel 3.38 to 4.17 μ)

Figure 21 is a block diagram of the two-color system dictated by feature graph considerations. The voltage in the signal channel is squared and amplified. The squared output is then compared to the voltage in the color channel. If the color channel voltage is larger than the squared output, background is indicated. If the reverse is true, a target is indicated. The variable gain amplifier is included to allow the setting of the constant k_1. For the data shown, $k_1 = 2.6 \times 10^4$ is the proper value; but this constant should be determined experimentally during the hardware phase of this project. Accurate calculation of its value is subject to various assumptions involving the detector characteristics; its determination by experiment should prove to be more reliable.

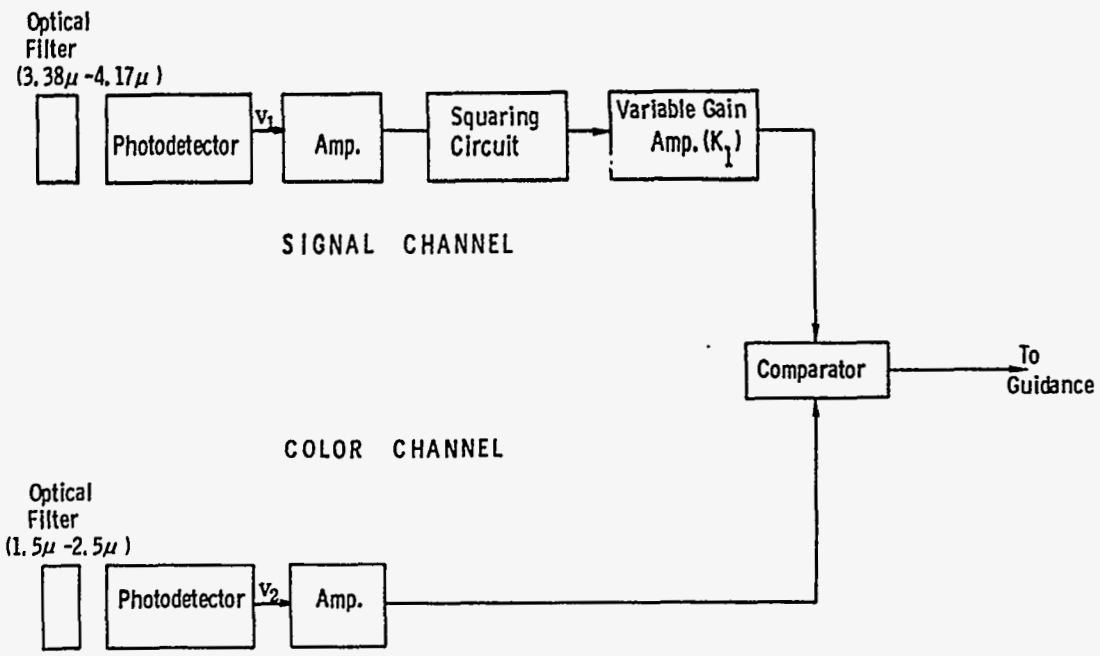

Figure 21. Block diagram of two-color discrimination system

These computations are based upon the only background spectral data known to the author. Should these data prove not to be representative, different signal processing functions may be indicated. The importance of obtaining additional experimental data is apparent. Further impetus for experiment is found in the realization that other wavelength regions, e.g., 8 to 14 μ or visible, might yield even farther separation on the feature graph. These possibilities can be assessed after the collection of spectrally resolved background data in these regions.

Other detection schemes based on pulse amplitudes can also be devised. For example, if an AGC system is used to drive the slowly varying components of the

detector voltages to a common value, a network can be designed to detect fast changes in the voltage in the two channels. If a pulse arises as a result of the scanning system encountering the sharp edge of a background transition, the amplitude of the pulse will be greater in the color channel than in the target channel. If, however, the pulse arises because of the presence of a target, the pulse amplitude (above the AGC level) in the signal channel will always be greater than that in the background channel. A threshold for this transcendence can be set for positive target identification. This threshold level will probably have to be determined by experiment. There are some instances, e.g., going from a snow background to a blue sky background, where the signal channel voltage may increase while the color channel voltage decreases. To prevent a false alarm in this case, it may be necessary to require that the direction of change in the two signals be the same for target identification. It appears that most of the other situations can be handled with the threshold level setting. While this is not intended as a complete analysis, it is useful in pointing out the proper direction to take in hardware implementation of this scheme. The following features are required:

1. AGC in both channels
2. Slope detector in both channels to ensure that a target is not identified unless both signals have the same slope
3. Threshold logic placed on the ratio of the pulse amplitudes of each channel.

This preliminary assessment indicates that the two-color discrimination technique can effectively discriminate against the background radiances given in Reference 11 for an aircraft in the nominal maneuver. Signal processing logic involves a simple squaring circuit.

More background data are needed to verify the computations and to allow investigation of additional spectral intervals.

Conclusions

Acquisition ranges for both the airfield denial task and the submarine defense task are adversely affected by the presence of background clutter. Modification of the present optical system to effect a decrease in the elemental field-of-view

by a factor of 3 will alleviate the problem; however, this modification may require exceeding the state of the art in detector fabrication. AGC-type detector logic is a minimum requirement for successful system operation, and it is likely that pulse length discrimination and/or two-color discrimination will also be required to effectively reduce the deleterious effects of background clutter.

For a single-channel system, the 3 to 5 μ spectral region appears optimum in that the target radiance is high, the atmospheric transmission is good, and the background radiance at its lowest value in this interval. For a two-color system, a spectral interval [1.5 μ, 2.5 μ] is recommended for the color channel, and the interval [3.38 μ, 4.17 μ] is recommended for the signal channel. This recommendation is based upon an analysis of the available background data in the 1.5 to 5.4 μ spectral region. Additional background data, spectrally resolved, are needed to allow investigation of other spectral regions.

In the airfield denial task, the target is easily acquired if the aircraft is using an afterburner. In this case, AGC-type logic is sufficient to provide acquisition probabilities in excess of 0.98 for all but a very few of the emplacement points. Maneuvers included in this category are low-fast, spiral, and maximum climb. For a false alarm probability of 10^{-6}, an S/N of 16.9 dB will yield an acquisition probability of 0.98. S/N values at acquisition time (1.1 sec after missile launch) range from 35 to 76 dB for the low-fast maneuver, 25 to 82 dB for the maximum climb maneuvers, and up to 60 dB for the spiral maneuver; these depend upon the location of the missile in the emplacement footprint. No discrimination, other than AGC is required.

Aircraft performing maneuvers at military power or cruise power are difficult to acquire. AGC-type logic is not sufficient for a majority of the points in the emplacement grid. Successful operation of the system against the low-slow and nominal maneuvers therefore requires very effective background discrimination techniques. With perfect discrimination, S/N values range from 14.9 to 59 dB for the low-slow maneuver and from 20.8 to 75 dB for the nominal maneuver. Effective discrimination is required for all points in the emplacement footprints which have cross ranges in excess of 250 meters.

The submarine defense task also requires effective background discrimination techniques. Elimination of background clutter will allow acquisition of helicopters at a range of 4.5 km.

Successful system operation is not limited by missile dynamics but rather by the acquisition capabilities of the infrared system. Therefore, further work on this project should be centered around the development of a sensor system with adequate bakcground discrimination capabilities.

APPENDIX A

Derivation of Signal-to-Noise Ratio Equation

INTENTIONALLY LEFT BLANK

APPENDIX A

Derivation of Signal-to-Noise Ratio Equation

The model describing the infrared acquisition system performance in this report is the same as that used by Mundie of the Rand Corporation. Reference 3 gives a derivation of the proper equation for S/N; however, a parallel derivation will be included here for completeness. Two cases are of interest. In the first case, the system will be assumed to be detector noise limited, i.e., background clutter will not be considered. Then, the effects of background clutter will be introduced and the resulting S/N equation given.

A. Detector-Noise-Limited Case

Infrared detectors are normally described by a term called NEP (Noise-Equivalent Power). NEP is the radiant flux incident on the detector surface necessary to give an output signal equal to the detector noise. The spectral NEP of an IR detector of area A_d and spectral detectivity D^*_λ is given by[13]

$$NEP(\lambda) = \frac{(A_d \Delta f)^{1/2}}{D^*_\lambda} \quad \text{(watts)} \qquad \text{(A-1)}$$

where Δf is the bandwidth of the electrical circuit employed. This quantity may be expressed in terms of the flux density at the entrance aperture (spectral noise equivalent flux density) as

$$NEFD(\lambda) = \frac{NEP(\lambda)}{T_o(\lambda) A_c} \quad \left(\frac{\text{watts}}{\text{cm}^2}\right). \qquad \text{(A-2)}$$

Here $T_o(\lambda)$ is the spectral transmittance of the optical system and A_c is the area of its collecting aperture.

The electrical bandwidth required in the detector depends upon the scan rate of the system. The output pulse from a detector scanning a point target will be approximately rectangular (apart from blur circle considerations). The system bandwidth

should be approximately one-half the reciprocal of the pulse width to produce a recognizable pulse at the output of the band-pass filter.[20] Therefore,

$$\Delta f T_d = 0.5 \tag{A-3}$$

where T_d, the dwell time, depends upon the scan rate and detector field-of-view. From one-dimensional considerations it can be shown that[1]

$$T_d = \frac{\theta_T}{2\pi N} \tag{A-4}$$

where θ_T is the acceptance angle of the optical system in the scan direction in radians, and N is the scan rate in revolutions per second. The angle θ_T is determined by the detector width, x_d, in the scan direction and the focal length of the optical system, f, as $\theta_T \cong x_d/f$. Therefore,

$$\Delta f = \frac{\pi f N}{x_d} . \tag{A-5}$$

For the system considered here,

$$x_d = 5.08 \times 10^{-3} \text{ cm}$$

$$f = 2.54 \text{ cm}$$

and $\Delta f = 1.57 \times 10^4$ Hz for a 10-rps roll rate.

It is now expedient to introduce the optical solid angle field-of-view, ω, of each elemental detector as[13]

$$\omega = \frac{A_d}{f^2} . \tag{A-6}$$

Combining Eqs. (A-1), (A-2), and (A-6) yields

$$NEFD(\lambda) = \frac{f\sqrt{\omega \Delta f}}{D^*_\lambda T_o(\lambda) A_c \eta} \quad \left(\frac{\text{watts}}{\text{cm}^2}\right) \tag{A-7}$$

where η has been introduced as an efficiency factor placed on the collection area, A_c. This factor will vary as the square of the cosine of the angle between the

target and the optical axis of the acquisition system. Equation (A-7) gives the amount of irradiance required at the photosurface of the detector to produce the detector-generated electrical noise which is present at the detector output terminals. It is the quantity which must be compared with the target irradiance to determine S/N.

The target spectral radiant intensity is denoted by $J_T(\lambda)$ (watts/sr-μ). Therefore, the spectral irradiance at the acquisition system caused by the presence of the target at range R is[13]

$$H_T(\lambda) = \frac{J_T(\lambda)T_A(\lambda)}{R^2} F(\lambda) \quad \left(\frac{\text{watt}}{\text{cm}^2\text{-}\mu}\right). \tag{A-8}$$

In this equation, $T_A(\lambda)$ is the atmospheric transmission between source and receiver and is a function of wavelength, and $F(\lambda)$ is the transmission function of the optical filter used ahead of the IR sensor. $J_T(\lambda)$ includes the effects of target aspect angle.

The signal-to-noise ratio for the detector noise limited case is then given:

$$\frac{S}{N} = \int_{\lambda_1}^{\lambda_2} \frac{H_T(\lambda)d\lambda}{NEFD(\lambda)}$$

where $[\lambda_1, \lambda_2]$ are the limits of the optical bandpass. Substituting Eqs. (A-7) and (A-8) in the above equation yields

$$\frac{S}{N} = \frac{\eta A_c}{f\sqrt{\omega\Delta f}\, R^2} \int_{\lambda_1}^{\lambda_2} J_T(\lambda)T_a(\lambda)F(\lambda)D^*_\lambda T_o(\lambda)\, d\lambda\,. \tag{A-9}$$

B. Background-Clutter-Limited Case

Detector limited noise operation occurs only when the irradiance at the sensor arising from fluctuations in background is small compared with the NEFD. This situation may arise when the background is blue sky or when a calm ocean is observed in a direction away from the sun. However, in a practical system, a high degree of background discrimination must be employed to obtain operation at this level. Assume an extended background with apparent radiance N_b(watts/sr-cm^2) as seen from the sensor. If the elemental field-of-view of each detector is ω, an area ωR^2 of background in the target plane is effective in illuminating the sensor. Therefore, the

effective sensor irradiance from background is

$$H_b = \frac{N_b}{R^2}\omega R^2 = N_b\omega \quad \left(\frac{\text{watts}}{\text{cm}^2}\right) \qquad \text{(A-10)}$$

Now N_b will change as the sensor scans its pattern. In one scan; several levels of background irradiance can be found. Assume that a maximum value and a minimum value of background radiance are observed during the scan.[3] Denote these values as N_b^{max} and N_b^{min}. During one scan, the sensor irradiance might appear as shown in Figure A-1.

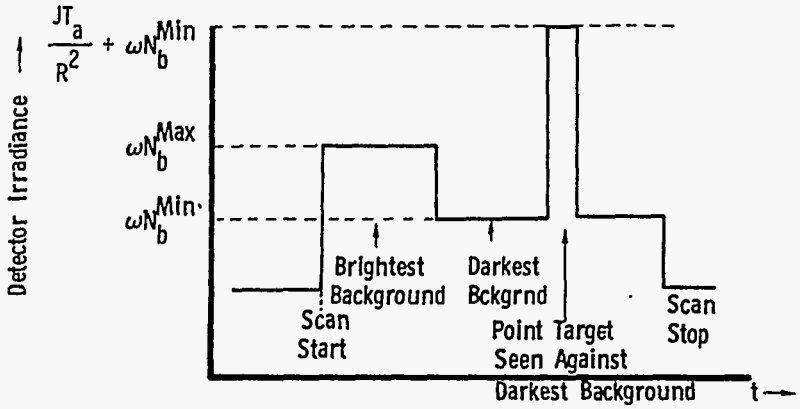

Figure A-1. Idealized description of detector irradiance for one scan (after Reference 3)

Sensor performance must then be determined by the amount, in relation to the NEFD, by which the minimum signal generated by the target ($J_T T/R^2 + \omega N_b^{min}$) exceeds the maximum background signal (ωN_b^{max}). Therefore, the effective signal arriving at the sensor must be reduced by the amount of background. If the signal level, $[J_T(\lambda)T_a(\lambda)F(\lambda)/R^2]$, in Eq. (A-8) is replaced by

$$F(\lambda)\left\{\frac{J_T(\lambda)T_a(\lambda)}{R^2} - \omega\left[N_\lambda(\text{max}) - N_\lambda(\text{min})\right]\right\} ,$$

and if this is used in Eq. (A-7) it would seem that the correct expression evolves. (Here N_λ is the background spectral radiance in w/sr - cm^2-μ.) However, Mundie reasons that to include the worst possible case the replacement ought to be

$$F(\lambda)\left\{\frac{J_T(\lambda)T_a(\lambda)}{R^2} - 2\omega\left[N_\lambda(\max) - N_\lambda(\min)\right]\right\}.$$

The additional factor of 2 is needed if the target is to be detected by simple threshold circuitry in which the threshold level is determined by the average background level established during one scan (narrow band AGC). Target irradiance must exceed this average value by a sufficient amount to prevent false alarms, and this requires the factor of 2. It is more general to let this effect be handled by a factor D, the discrimination factor, and write the effective sensor irradiance as

$$F(\lambda)\left\{\frac{J_T(\lambda)T_a(\lambda)}{R^2} - D\omega\left[N_\lambda(\max) - N_\lambda(\min)\right]\right\}.$$

When D = 2, a narrow band AGC is implied. D can approach unity if proper background discrimination techniques are employed. For example, when (wide band) AGC-type logic is employed, the threshold level can be allowed to vary as the background radiance changes. In this case, D = 1 is the proper value. The discrimination factor concept allows direct comparison of the effects of various discrimination techniques on the S/N ratio. For perfect discrimination, D is zero and the detector noise limited S/N is obtained. Note also that, if the background is uniform, i.e., $N_\lambda(\max) = N_\lambda(\min)$, the system again operates at the detector noise limit.

The signal-to-noise ratio for background limited operation can then be expressed as

$$\frac{S}{N} = \frac{\eta A_c}{f\sqrt{\omega\Delta f}}\int_{\lambda_1}^{\lambda_2}\left\{\frac{J_T(\lambda)T_a(\lambda)}{R^2} - D\omega\left[N_\lambda(\max) - N_\lambda(\min)\right]\right\}D_\lambda^* T_o(\lambda)F(\lambda)\,d\lambda. \qquad \text{(A-11)}$$

This is the equation which has been evaluated in this report.

[redacted]

UNCLASSIFIED

INTENTIONALLY LEFT BLANK

UNCLASSIFIED

[redacted]

APPENDIX B

Detection Probability Equations

[redacted]

INTENTIONALLY LEFT BLANK

[redacted]

APPENDIX B

Detection Probability Equations

Quantum noise in photodetectors is usually described by Gaussian statistics.[13] It is the tendency of some authors to describe the detection probability of a scanning IR system in terms of Rayleigh statistics. The Rayleigh description of noise is correct only when a carrier system is used, e.g., video detection of radar signals and detection of IR signals by reticle trackers. For a carrier system with threshold detection, curves of detection probability as a function of S/N ratio may be found in many radar handbooks.[21] However, if the search set is not a carrier system, no nonlinear process is involved in signal detection. Therefore, the output noise should be considered to be distributed normally.[22]

The probability that a noise pulse alone will exceed the bias or threshold level, y, is given by

$$P_{fa} = \frac{1}{\sqrt{2\pi}} \int_{y}^{\infty} \exp(-u^2/2)\, du \,. \qquad \text{(B-1)}$$

False alarm probability can also be expressed in terms of the time between false alarms, τ_{fa}, as[13]

$$P_{fa} = \frac{1}{\tau_{fa} \Delta f} \,. \qquad \text{(B-2)}$$

The maximum flight time of the SIAM missile system is 22 seconds. If a time between false alarms of 100 seconds and a bandwidth of approximately 10^4 are assumed, the false alarm probability can be seen to be 10^{-6}. In order to determine the setting of the threshold voltage above the noise voltage, Eq. (B-1) may be equated to 10^{-6}, i.e.,

$$\frac{1}{\sqrt{2\pi}} \int_{y}^{\infty} \exp(-u^2/2)\, du = 10^{-6} \,. \qquad \text{(B-3)}$$

Inspection of tables of normal percentile points[23] indicates that this equation is solved for a value of y of 4.75. This means that the threshold voltage level should

be 4.75 times as high as the detector noise level to give 10^{-6} probability of false alarm. If the threshold is set higher, P_{fa} decreases in accordance with Eq. (B-1).

The acquisition probability is now determined by the amount by which the S/N ratio exceeds the threshold value. The proper equation is[22]

$$P_a = \frac{1}{\sqrt{2\pi}} \int_{(y-S/N)}^{\infty} \exp(-t^2/2)\, dt \,. \qquad \text{(B-4)}$$

This equation may also be expressed as

$$P_a = \frac{1}{2} \operatorname{erfc}\left(\frac{y - S/N}{\sqrt{2}}\right) . \qquad \text{(B-5)}$$

In this report, y has been set at 4.75, and Eq. (B-5) has been used in computing acquisition probabilities.

APPENDIX C

Equations for Target Pulse Width

INTENTIONALLY LEFT BLANK

APPENDIX C

Equations for Target Pulse Width

Point targets are imaged by optical systems as blur circles with finite diameters. A true point image would yield a rectangular signal pulse with time duration equal to the system dwell time. In that the image is not a point, the temporal characteristics of the target pulse generated by the scanning detector are not rectangular. Instead, pulse shape is determined by the convolution of the scanning detector area with the blur circle of the target image.

The temporal behavior of the output pulse is described by[18]

$$p(t) = \int_{-\infty}^{\infty} \int_{-\infty}^{\infty} h_I(\dot{x}t - x,y)\, A_d(x,y)\, dy\, dx \qquad \text{(C-1)}$$

where

$h_I(x,y)$ = normalized blur energy in the image plane

$A_d(x,y)$ = detector area

$\dot{x}$ = velocity with which the detector is scanned across the blur image

Scanning is assumed to occur only in the x dimension. If x_d and y_d represent the detector dimensions, Eq. (C-1) may be written as

$$p(t) = \int_{t\dot{x}}^{(t+T_d)\dot{x}} dx \int_{-y_{d/2}}^{y_{d/2}} h_I(x,y)\, dy \qquad \text{(C-2)}$$

where

T_d = dwell time of a point image on the detector

$\dot{x} = x_d/T_d$.

The blur circle is described by a Gaussian distribution with a standard deviation radius denoted by σ. If zero mean is assumed, the energy distribution varies as

$$h_I(x,y) = K \exp\left[-\left(x^2+y^2\right)/2\sigma^2\right] \qquad \text{(C-3)}$$

where K is a constant.

Substituting Eq. (C-3) into Eq. (C-2) yields

$$p(t) = K\int_{t\dot{x}}^{\dot{x}(t+T_d)} \exp\left(-x^2/2\sigma^2\right) dx \int_{-y_{d/2}}^{y_{d/2}} \exp\left(-y^2/2\sigma^2\right) dy . \qquad \text{(C-4)}$$

Now

$$\frac{1}{\sqrt{2\pi}}\int_{-x}^{\dot{x}} \exp\left(-t^2/2\right) dt = \operatorname{erf}\frac{x}{\sqrt{2}} .$$

In Eq. (C-4) let $y^2/2\sigma^2 = t^2/2$ and integrate over y. This gives

$$p(t) = K\sigma\sqrt{2\pi}\ \operatorname{erf}\left(\frac{y_d}{2^{3/2}\sigma}\right)\int_{\dot{x}t}^{\dot{x}(t+T_d)} \exp\left(-x^2/2\sigma^2\right) dx . \qquad \text{(C-5)}$$

Equation (C-5) may be written as

$$p(t) = \left(K\sqrt{2\pi}\ \sigma\right) \operatorname{erf}\left(\frac{y_d}{2^{3/2}\sigma}\right)\left[\int_o^{\dot{x}(t+T_d)} \exp\left(-x^2/2\sigma^2\right) dx - \int_o^{\dot{x}t} \exp\left(-x^2/2\sigma^2\right) dx\right]. \qquad \text{(C-6)}$$

Again utilizing a change of variable, the result may be shown to be

$$p(t) = K\pi\sigma^2 \operatorname{erf}\left(\frac{y_d}{2^{3/2}\sigma}\right)\left\{\operatorname{erf}\left[\frac{\dot{x}\left(t+T_d\right)}{\sqrt{2}\,\sigma}\right] - \operatorname{erf}\left(\frac{\dot{x}t}{\sqrt{2}\,\sigma}\right)\right\}. \qquad \text{(C-7)}$$

The normalized version of Eq. (C-7) has been plotted in Figure 16.

References

1. J. M. McIntire and G. A. Kinemond, The Little David Acquisition Problem--A Preliminary Feasibility Study (U), Sandia Laboratories Report SLA-73-0547, May 1973 (SNSI).

2. G. S. Bennett, Little David Dynamics Analysis, Sandia Laboratories Report (to be published).

3. L. G. Mundie, Passive Target-Acquisition Sensors for Laser Systems (U), Rand Report R-730-ARPA, July 1971 (SNSI).

4. General Dynamics, Redeye Advanced Sensor Development Program (ASDP) Phase IV, Target Signature Measurements, Final Report, Report CR-6-125-830-001, November 1970 (SNSI).

5. General Dynamics, Infrared Signature Evaluation of a CH-47C Helicopter, Report TM6-125PH-341, Vol. I, January 1972 (SNSI).

6. Defense Intelligence Agency, Fishbed Weapon System (U), ST-CS-09-31-69, February 6, 1970 (SDI).

7. J. E. A. Selby and R. A. McClatchey, Atmospheric Transmittance from 0.25 to 28.5 μm: Computer Code Lowtran 2, AFCRL-72-0745, December 1972.

8. A. Arnulf, J. Bricard, E. Cure, and C. Veret, "Transmission by Haze and Fog in the Spectral Region 0.35 to 10 Microns," Jour. Opt. Soc. Am., 47, No. 6, pp. 491-498, June 1957.

9. S. W. Kurnick, R. N. Zitter, and D. B. Williams, "Attenuation of Infrared Radiation by Fogs," Jour. Opt. Soc. Am., 50, No. 6, pp. 578-583, June 1960.

10. D. M. Gates and C. C. Shaw, "Infrared Transmission of Clouds," Jour. Opt. Soc. Am., 50, No. 9, pp. 876-882, September 1960.

11. G. W. Ashley, D. W. Blay, E. O. Buenting, and A. G. Tescher, "Spectral Contrast of Backgrounds Between 1.5 and 5.4 Micrometers" (U), Proc. IRIS, NAVSOP 2315V, Vol. 14, No. 1, February 1970 (SNSI).

12. G. R. Aroyan, "The Technique of Spatial Filtering," Proc. Inst. Radio Engrs., Vol. 47, No. 9, pp. 1561-1568, September 1959.

13. R. D. Hudson, Infrared System Engineering, Wiley-Interscience, John Wiley and Sons, New York, 1969.

14. W. L. Wolfe, Handbook of Military Infrared Technology, Superintendent of Documents, U. S. Government Printing Office, Washington, D.C., 1965.

15. N. M. Worthy, et al., First Quarterly Report on Advanced Development Task IV, IR Surveillance (U), The Aerojet-General Corporation, AZ67-00712(3207), May 1967 (SNF).

16. Flight Test Program on Infrared Track-While-Scan System (U), The AVCO Corporation, Report AFAL-TR-65-24, March 1965 (Secret).

17. D. Green, et al., Airborne Applications Study: Vol. 2, System Concept Description (U), Hughes Aircraft Co., AFWL-TR-69-125, October 1969 (SRD).

[redacted]

[redacted]

INTENTIONALLY LEFT BLANK